1 **Endocrine disruptor-induced epimutagenesis *in vitro*: Insight into molecular mechanisms**

2 Jake D. Lehle, Yu-Huey Lin, Amanda Gomez, Laura Chavez, and John R. McCarrey*

3 Department of Neuroscience, Developmental and Regenerative Biology

4 The University of Texas at San Antonio

5

6 *Corresponding author – John R. McCarrey, john.mccarrey@utsa.edu

7 **Keywords**: Endocrine disrupting chemicals, epigenetics, DNA methylation, epigenetic reprogramming,

8 transgenerational epigenetic inheritance

9

10 **Abstract:**

11 Endocrine disrupting chemicals (EDCs) such as bisphenol S (BPS) are xenobiotic compounds that can

12 disrupt endocrine signaling following exposure due to steric similarities to endogenous hormones within

13 the body. EDCs have been shown to induce disruptions in normal epigenetic programming

14 (epimutations) that accompany dysregulation of normal gene expression patterns that appear to

15 predispose disease states. Most interestingly, the prevalence of epimutations following exposure to

16 many different EDCs often persists over multiple subsequent generations, even with no further

17 exposure to the causative EDC. Many previous studies have described both the direct and prolonged

18 effects of EDC exposure in animal models, but many questions remain about molecular mechanisms by

19 which EDCs initially induce epimutations or contribute to the propagation of EDC-induced epimutations

20 either within the exposed generation or to subsequent generations. Additional questions remain

21 regarding the extent to which there may be differences in cell-type specific susceptibilities to various

22 EDCs, and whether this susceptibility is correlative with expression of relevant hormone receptors

and/or the location of relevant hormone response elements (HREs) in the genome. To address these questions, we exposed cultured mouse pluripotent (induced pluripotent stem [iPS]), somatic (Sertoli and granulosa), and germ (primordial germ cell like [PGCLC]) cells to BPS and measured changes in DNA methylation levels at the epigenomic level and gene expression at the transcriptomic level. We found that there was indeed a difference in cell-type specific susceptibility to EDC-induced epimutagenesis and that this susceptibility correlated with differential expression of relevant hormone receptors and, in many cases, tended to generate epimutations near relevant HREs within the genome. Additionally, however, we also found that BPS can induce epimutations in a cell type that does not express relevant receptors and in genomic regions that do not contain relevant HREs, suggesting that both canonical and non-canonical signaling mechanisms can be disrupted by BPS exposure. Most interestingly, we found that when iPS cells were exposed to BPS and then induced to differentiate into PGCLCs, the prevalence of epimutations and differentially expressed genes (DEGs) initially induced in the iPSCs was largely retained in the resulting PGCLCs, however, >90% of the specific epimutations and DEGs were not conserved but were rather replaced by novel epimutations and DEGs following the iPSC to PGCLC transition. These results are consistent with a unique concept that many EDC-induced epimutations may normally be corrected by germline and/or embryonic epigenetic reprogramming but that due to disruption of the underlying chromatin architecture induced by the EDC exposure, many novel epimutations may emerge during the reprogramming process as well. Thus, it appears that following exposure to a disruptive agent such as an EDC, a prevalence of epimutations may transcend epigenetic reprogramming even though most individual epimutations are not conserved during this process.

Introduction

45 It has now been more than a half-century since Roy Hertz in 1958 first proposed the notion that
46 certain chemicals, particularly those used in livestock feed at the time, could contaminate food sources
47 and bioaccumulate in humans mimicking the activity of hormones (Gassner et al., 1958). As the number
48 of potential chemicals that could exert these effects has grown, so too has the interest in this area to the
49 point that this is now a major topic of active research. The dangers of many endocrine disrupting
50 chemicals (EDCs) studied to date have largely been investigated utilizing animal models. A primary
51 example is the multi-phased Toxicant Exposures and Responses by Genomic and Epigenomic Regulators
52 of Transcription (TaRGET) program established to determine the contribution of environmental
53 exposures to disease pathogenesis as a function of epigenome perturbation in mouse models (Wang et
54 al., 2018). While the use of animal models has been quite informative for determining the various
55 systemic or organ/tissue-specific disease-related effects associated with exposure to different EDCs, the
56 molecular mechanisms underlying these phenomena remain poorly understood. Thus, questions persist
57 regarding i) the mechanisms by which exposure of cells to EDCs results in the initial formation of
58 epimutations defined here as any change in epigenomic programming, ii) potential cell-type specific
59 differential susceptibility to epimutagenesis induced by different EDCs, iii) the potential involvement of
60 relevant hormone receptors and/or genomic hormone response elements in EDC-induced disruption of
61 the epigenome, and iv) the ability of an EDC-induced epimutated state to persist inter- or
62 transgenerationally despite generational epigenetic reprogramming (Diaz-Castillo et al., 2019).

63 Questions about molecular mechanisms responsible for EDC-exposure based disruption of
64 normal epigenetic programming have been difficult to interpret in whole animal models due, in part, to
65 the inherent complexity of the intact animal including potential interactions among multiple different
66 organs, tissues, and cell types at the paracrine, metabolic and/or systemic levels. To circumvent this
67 challenge, we opted to expose homogeneous populations of specific cell types in culture to doses of the
68 EDC, BPS, that are below the maximum safe limit previously set by the EPA for exposure of humans to

69 the similar estrogen mimetic, BPA. In this way we hoped to learn more about the manner in which direct
70 exposure to a specific EDC induces epimutations and differential gene expression in different individual
71 cell types including somatic cells, pluripotent cells, and germ cells. This approach was designed to
72 distinguish the direct effects of an EDC exposure *in vitro* from indirect effects that may accrue as the
73 result of an EDC exposure on one cell type inducing a secondary effect on a neighboring or related cell
74 type *in vivo*.

75 Previous *in vitro* studies have demonstrated direct susceptibility of cultured cell types to EDC-
76 induced epimutagenesis, however, those studies were focused on immortalized cancer cell lines that do
77 not necessarily model key cell types involved in normal initial incursion or subsequent intragenerational
78 propagation or inter- or transgenerational transmission of environmentally-induced epimutations *in vivo*
79 (Deb et al., 2016; Goodman et al., 2014; Huang et al., 2019; Karaman and Ozden, 2019; Senyildiz et al.,
80 2017). We chose to examine direct exposure of three key types of cells relevant to environmental
81 exposures and subsequent propagation and transmission of induced epimutations *in vivo* – somatic cell
82 types known to be responsive to endocrine signaling (Sertoli cells and granulosa cells), pluripotent cells
83 mimicking the preimplantation embryo (iPSCs), and germline cells (PGCLCs).

84 While there have been reports that have clearly indicated the ability of EDCs to disrupt classical
85 endocrine signaling (Henley and Korach, 2010; Kelce et al., 1995; Swedenborg et al., 2009; vom Saal and
86 Hughes, 2005; You et al., 1998), there exist other reports indicating EDCs can also disrupt non-classical
87 endocrine signaling via nuclear receptors (Ozgyin et al., 2015; Song et al., 2011), G protein-coupled
88 receptors (Thomas and Dong, 2006), and calcium channel signaling (Brenker et al., 2018). This has
89 further complicated our understanding of the mechanism(s) by which EDC exposure initially induces
90 epimutations, and has particularly confounded insight into the susceptibility of germ cells to EDC-
91 induced epimutagenesis given that germ cells are reported to lack expression of classical endocrine
92 receptors (Meccariello et al., 2014). This is relevant to the effort to understand mechanisms underlying

93 transgenerational epigenetic inheritance of EDC-induced epimutations (Anway et al., 2006; Guerrero-
94 Bosagna et al., 2012; Nilsson et al., 2008) which clearly implicates transmission via the germ line.

95 The concept of germline transmission of EDC-induced epimutations is further confounded by the
96 known epigenetic reprogramming events that occur in the preimplantation embryo and developing fetal
97 and neonatal germ line. Thus, regardless of how EDC-induced epimutations become initially manifest in
98 the germ line, it is not clear how they subsequently persist and are transmitted inter- or
99 transgenerationally given the large portion of the epigenome that undergoes genome-wide erasure and
100 resetting of epigenetic programming during each generation (Cantone and Fisher, 2013; Lee et al., 2014;
101 Santos et al., 2002; Sanz et al., 2010). *In vitro* cell culture systems afford the opportunity to focus on
102 individual cell types independently, including somatic cells which are likely initially exposed to most
103 environmental disruptive influences, pluripotent cells which represent the preimplantation embryo in
104 which the first major reprogramming event occurs during normal development, and early germline cells
105 where the second major reprogramming event is initiated in primordial germ cells (PGCs). Importantly,
106 in addition to the potential to study each of these cell types independently, it is possible to induce
107 transitions in cell fate *in vitro* that model those that occur during normal development, thereby
108 recapitulating normal reprogramming events in a way that can facilitate high resolution studies of the
109 fate of EDC-induced epimutations once they have been induced in any of these cell types.

110 Here we describe our study of the relative susceptibility to induction of epimutations by direct
111 exposure of four different cell types maintained in culture – somatic Sertoli and granulosa cells,
112 pluripotent iPSCs, and germ line PGCLCs – to BPS, followed by our analysis of the fate of epimutations
113 initially induced in mouse iPSCs that are then induced to transition into PGCLCs. We found that there are
114 cell-type specific differences in susceptibility to epimutagenesis and associated dysregulation of gene
115 expression patterns following exposure of these different cell types to a similar dose of BPS below the
116 maximum safe limit established by the EPA for exposure of human cells to BPA (Ribeiro et al., 2019). We

117 further found that BPS induction of epimutations in both pluripotent and somatic cell types that express
118 relevant estrogen receptors (ERs), as well as in germ cells which do not express ERs, suggests disruption
119 of both canonical and non-canonical endocrine signaling. Most interestingly, we found that when iPSCs
120 exposed to BPS were then induced to undergo a major transition in cell fate and related epigenetic
121 reprogramming to form PGCLCs, a similar prevalence of epimutations and DEGs was retained, but,
122 surprisingly, very few (<10%) specific epimutations or DEGs were conserved during this process. This
123 suggests that the initial EDC exposure induces disruption of the chromatin landscape that subsequent
124 epigenetic reprogramming is unable to fully restore. Thus, reprogramming during a major cell fate
125 transition appears to correct many of the initially induced epimutations, but also appears to induce
126 many *de novo* epimutations, and this imbalance may persist across multiple generations which may
127 contribute to continued transgenerational epigenetic inheritance of EDC-induced phenotypes during
128 succeeding generations.

129

130 **Results**

131 **Dose dependent epimutagenesis response to BPS exposure in iPSCs**

132 To initially assess the extent to which epimutations and dysregulated gene expression can be
133 induced in cells maintained in culture, we exposed mouse iPSCs to three doses of BPS (1, 50, and 100
134 μM) and measured the impact on the epigenome and transcriptome using the Illumina Infinium Mouse
135 Methylation BeadChip Array and RNA-seq, respectively (Figure 1). All three doses of BPS induced
136 individual differentially methylated CpGs (DMCs) as well as differentially methylated regions (DMRs)
137 (Figure 1a, Supplement tables 1 and 2), and differentially expressed genes (DEGs) (Figure 1b,
138 Supplement table 3) when compared to control mouse iPSCs treated with vehicle (EtOH) only. The
139 extent of this exposure-specific epimutagenesis was correlated with the dose of BPS used. Information

140 regarding the number and overlap of DMCs/DMRs/DEGs identified for each dose of BPS is shown in
141 Supplement tables 1-4 and Supplement figure 1. Importantly, in many cases we observed a correlation
142 between differential expression of a gene and the presence of DMCs in the promoter region of that
143 gene (Supplement figure 2). These results provided an initial proof of concept that exposure of cells
144 maintained *in vitro* to an EDC such as BPS can disrupt the epigenome and transcriptome in a dose-
145 dependent manner. Interestingly, exposure to 1 µM BPS induced very few DMRs, but did induce
146 widespread DMCs and DEGs. Because 1 µM BPS is below the FDA's suggested safe environmental level
147 established for exposure of humans or intact animals to BPA (Ribeiro et al., 2019), and was sufficient to
148 induce DMCs and dysregulated gene expression on all chromosomes in our cultured iPSCs, we utilized
149 this dose and focused solely on DMCs when assessing epimutations in all subsequent experiments.

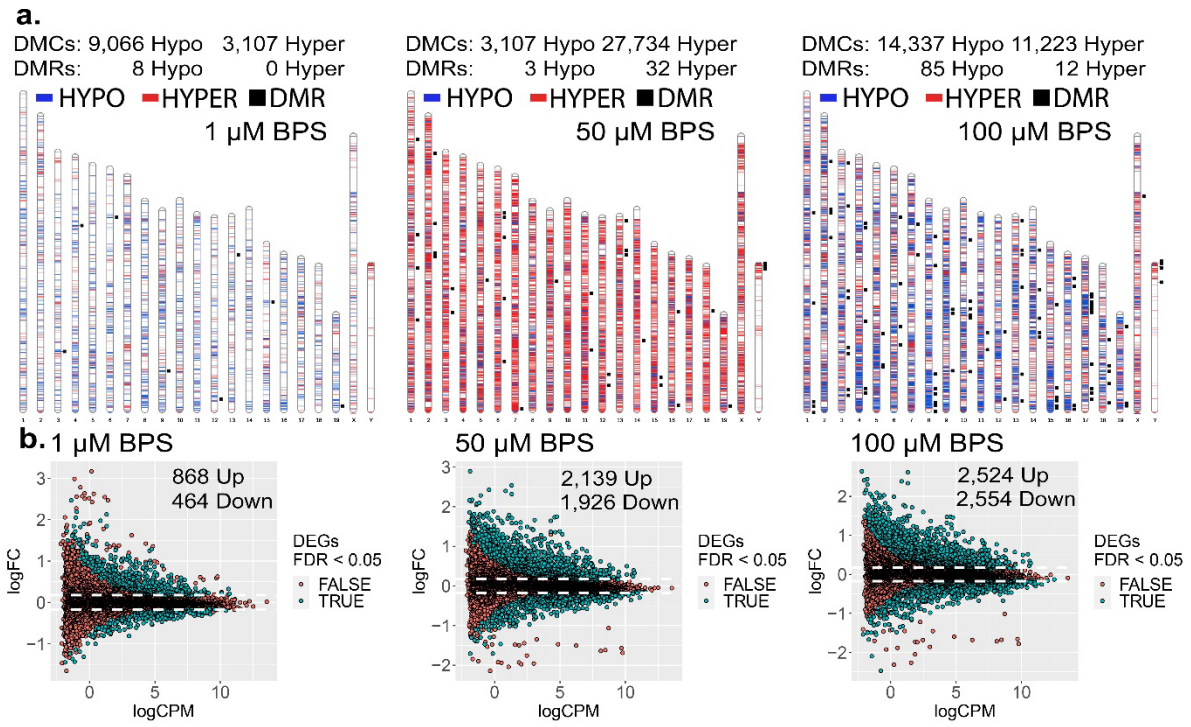

150

151 **Figure 1. Dose dependent impact of epimutagenesis measured in iPSCs exposed to 1, 50, and 100 µM**
152 **BPS. a)** Ideogram plots displaying chromosomal distribution of genome-wide changes in DNA
153 methylation caused by BPS exposure. **b)** Mean difference (MD) plots of changes in gene expression
154 following exposure to increasing doses of BPS. Exposure to increasing doses of BPS induced increasing,
155 although plateauing numbers of DMCs, DMRs, and DEGs. Blue horizontal lines = hypomethylated DMCs,
156 red horizontal lines = hypermethylated DMCs, black squares = DMRs.

157

158

159 **Cell-type specific susceptibility to induction of epimutations following BPS exposure**

160 We next sought to determine if different key cell types – somatic, pluripotent or germ – are
161 differentially susceptible to induction of epimutations in response to direct exposure of each to a similar
162 dose of BPS. Thus, we exposed pluripotent (iPSCs), somatic (Sertoli and granulosa cells), and germ
163 (PGCLCs) cell types to 1 µM BPS and measured changes in DNA methylation patterns. We identified
164 exposure-specific DMCs in each exposed cell type relative to its corresponding control (exposed to
165 carrier only) (Figure 2a). We observed overall differences among the different cell types in total numbers
166 of DMCs, with iPSCs showing the highest number of DMCs, followed by Sertoli cells and granulosa cells,
167 and then PGCLCs, respectively (Table 1).

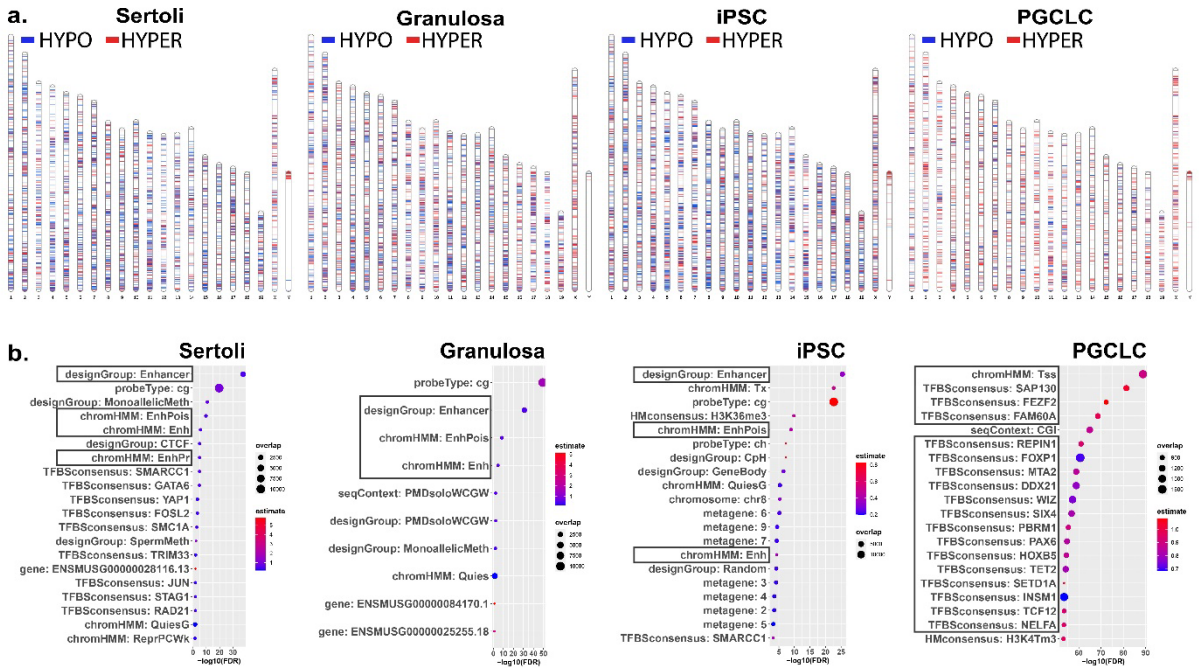

168

169 **Figure 2. Chromosomal distributions and annotations of BPS-induced epimutations in pluripotent,**
170 **somatic, and germ cell types. a)** Ideograms illustrating chromosomal locations of DMCs induced by
171 exposure of each cell type to 1 µM BPS. Blue horizontal lines = hypomethylated DMCs, red horizontal
172 lines = hypermethylated DMCs. **b)** Enrichment plots indicating feature annotations in genomic regions
173 displaying prevalent BPS-induced epimutations in each cell type. Dot size = number of overlapping DMCs

174 with specific annotation, dot color = enrichment score reflecting the relative degree to which
175 epimutations occurring in a specific annotated class are overrepresented.

176

Table 1. Treatment-specific differentially methylated sites (DMCs) (treated vs. control)

DMCs	Sertoli	Granulosa	iPSCs	PGCLCs
Hypomethylated[1]	7,385	6,444	9,651	2,315
Hypermethylated[2]	3,022	4,143	4,308	4,785
Total	10,407	10,587	13,959	7,100

177 [1]A CpG site that was predominantly methylated in the control samples but unmethylated in the exposed samples.
178 [2]A CpG site that was predominantly unmethylated in the control samples but methylated in the exposed samples.

179

180 Interestingly, among the exposure-specific DMCs identified in each cell type, we observed
181 predominantly hypomethylated DMCs in the somatic and pluripotent cell types, but predominantly
182 hypermethylated DMCs in PGCLCs (Table 1). These findings confirm that there are both quantitative
183 differences among cell types in overall susceptibility to epimutagenesis, and qualitative cell-type specific
184 differences in the prevalence of hypo- versus hypermethylated DMCs following exposure to BPS. The
185 latter likely reflects the fact that the epigenome in PGCs is naturally more hypomethylated than that in
186 pluripotent or somatic cell types (Hajkova, 2011), enhancing the likelihood that most changes in DNA
187 methylation induced in PGCLCs will necessarily involve hypermethylation.

188 **Annotation of BPS-induced epimutations**

189 As we only found an average of 11.05% direct overlap in DMCs between two or more cell types
190 and no overlapping DMCs shared between all cell types (Supplement figure 1), we next analyzed
191 annotations associated with genomic sites of BPS exposure-specific DMCs in each cell type. We mined
192 annotations associated with genomic regions included on the Infinium array and found that a substantial
193 group of exposure-specific DMCs was associated with enhancer regions in the two somatic (Sertoli and

194 granulosa) and one pluripotent (iPS) cell types exposed to BPS, while in PGCLCs BPS-induced DMCs were
195 more prevalent at promoter regions containing transcription start sites (TSSs) and transcription factor
196 binding sites (Figure 2b), indicative of yet another qualitative cell-type specific difference in induction of
197 epimutations by the same dose of BPS.

198

199 **Relationship between susceptibility to BPS-induced epimutagenesis and expression of relevant**
200 **hormone receptors**

201 As EDCs are thought to induce epimutations via disruption of classical hormonal signaling
202 (Henley and Korach, 2010; Kelce et al., 1995; Swedenborg et al., 2009; vom Saal and Hughes, 2005; You
203 et al., 1998), we next sought to determine if the differential extent of BPS induction of epimutations we
204 observed in different cell types was associated with differential expression of relevant hormone
205 receptors in each. We performed immunocytochemistry (ICC) to detect the presence of the relevant
206 estrogen receptors – ERα and ERβ, while co-staining for cell-type specific markers (WT1 [Sertoli cell
207 marker], FSHR [granulosa cell marker], FUT4 [iPSC marker], and NANOG [PGCLC or endogenous PGC
208 marker]) to confirm the identity of the four cultured cell types examined in this study (Sertoli cells,
209 granulosa cells, iPSCs and PGCLCs), as well as endogenous mouse PGCs (Figure 3a). Both somatic cell
210 types (Sertoli and granulosa) showed positive immunolabeling for both ERα and ERβ, whereas the
211 pluripotent cells showed positive immunolabeling for ERβ, but negative immunolabeling for ERα, and
212 the PGCLCs and endogenous PGCs showed negative immunolabeling for both ERα and ERβ. Importantly,
213 the latter result is consistent with previous reports of lack of expression of either ERα or ERβ at the
214 protein level in endogenous PGCs (Meccariello et al., 2014).

215 These results demonstrate cell-type specific differences in expression of hormone receptors
216 (ERα and ERβ) which are potentially relevant to the disruptive action of the estrogen mimetic, BPS. We

217 noted that expression of at least one potentially relevant hormone receptor (ERβ) in either somatic or
218 pluripotent cells correlated with a higher incidence of DMCs induced by exposure of somatic or
219 pluripotent cell types to 1 μM BPS relative to the incidence of DMCs induced by exposure of PGCLCs,
220 which do not express either estrogen receptor, to the same dose of BPS (Table 1). Nevertheless, we did
221 still observe induction of DMCs when PGCLCs were exposed to BPS, demonstrating that expression of
222 relevant canonical hormone receptors is not an absolute requirement for induction of epimutations in
223 response to an EDC. To exclude the possibility that the observed susceptibility in germ cells could be
224 correlated with the presence of other endocrine receptors that could interact with BPS, we performed
225 additional ICC for the presence of AR, PPARγ, and RXRα and found they were all absent as well in
226 endogenous PGCs (Supplement figure 4). This result and our observation noted above that somatic and
227 pluripotent cell types showed a higher incidence of epimutations at apparent enhancer regions while
228 germ cells showed a higher epimutation incidence at apparent promoter regions reveal cell-type specific
229 differences in susceptibility to induction of epimutations by exposure to the EDC, BPS.

230 **Proximity of BPS-induced epimutations to genomic EREs**

231 The relatively higher incidence of BPS-induced epimutations in cell types expressing one or both
232 estrogen receptor(s) suggests BPS-induced epimutagenesis may be manifest, at least in part, through
233 canonical endocrine signaling pathways. If this is the case, we might expect to see elevated induction of
234 epimutations in genomic regions enriched for relevant HREs which, for interactions with the estrogen
235 mimetic, BPS, would be EREs. Previous studies have defined a full ERE consensus sequence (Bourdeau et
236 al., 2004), but other reports have indicated that estrogen receptors can often bind to ERE half-sites
237 (Mason et al., 2010) (Figure 3b). Indeed, when we mined publicly available ERα ChIP-seq peaks from the
238 UCSC genome browser database (Dunham et al., 2012; Myers et al., 2011; Sloan et al., 2016; Wang et
239 al., 2013, 2012) and performed motif enrichment, we identified two distinct ERE half-sites within regions

240 enriched for DMCs rather than one full sized ERE consensus sequence, with the half-sites appearing to
241 be more biologically relevant to interaction with estrogen or its mimetics (Figure 3b). We then plotted
242 the frequency of ERE half-sites in genomic regions within 500 bp of BPS-induced epimutations (Figure
243 3c,d). We found an increase in the frequency of ERE half-sites identified within 500 bp of BPS-induced
244 DMCs genome-wide in all four cell types investigated, but the frequency was notably lower in germ cells
245 (Figure 3c). Thus, this higher frequency of ERE half-sites within 500 bp of BPS-induced DMCs was
246 conserved in three of the four cell types – somatic (Sertoli and granulosa) and pluripotent (iPSCs) when
247 we focused solely on apparent enhancer regions, but not in germ cells (PGCLCs) where the majority of
248 DMCs occurred at apparent promoter regions (Figure 3d). We also mined the UCSC mouse genome
249 sequence for genome-wide prevalence of ERE half-sites and found that while these sites occur in both
250 promoter and enhancer regions, they are nearly four-fold more frequent in enhancers (Supplement
251 figure 5, Supplement table 5). Thus, it is perhaps not surprising that BPS-induced epimutations were
252 more prevalent in enhancer regions in somatic and pluripotent cell types that express one or both ERs,
253 than in germ cells that do not express either ER.

254

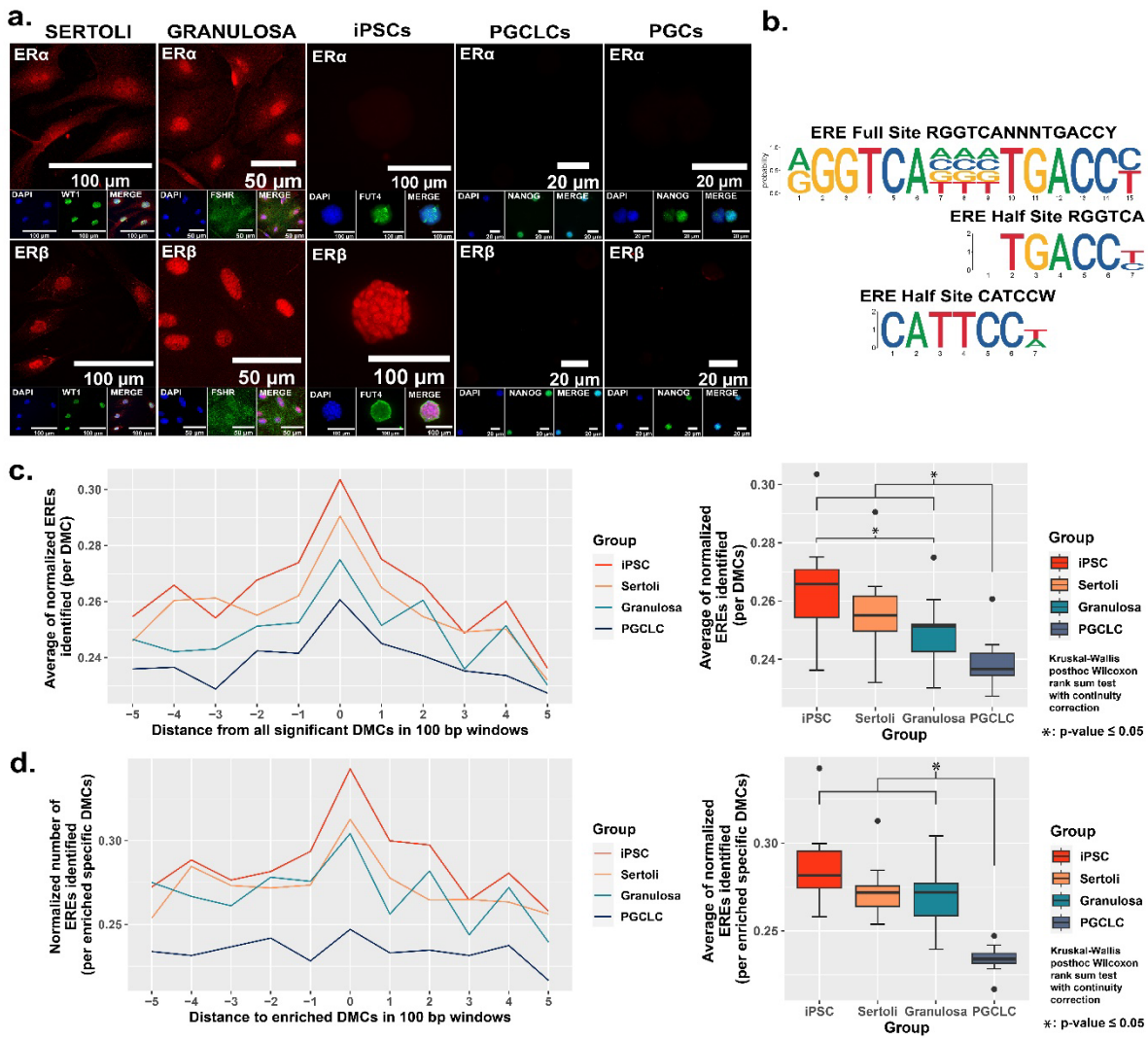

Figure 3. Correlation between cell-type specific expression of estrogen receptors and density of genomic EREs associated with BPS-induced epimutations. a) Assessment of expression of ERα and ERβ by cell types co-stained for known cell-type specific markers. Somatic cell types express both receptors, pluripotent cells express ERβ but not ERα, and germ cells do not express either estrogen receptor. **b)** Motif plots displaying the full ERE consensus sequence and the more biologically relevant ERE half-site motifs found to be enriched from ERα ChIP-seq. **c,d)** Normalized density plots and box plots displaying the frequency of ERE half-sites identified c) within 500 bp of all BPS-induced DMCs genome-wide, or d) within 500 bp of the most enriched categories of BPS-induced DMCs in each cell type (= enhancer regions for somatic and pluripotent cell types and promoter regions in the germ cell type).

Taken together, these results suggest a relationship between i) expression of either ERβ alone or ERα and ERβ together, ii) elevated susceptibility to BPS-induced epimutagenesis, and iii) the occurrence of BPS-induced DMCs in genomic regions – particularly enhancers – containing EREs. These observations

269 are consistent with the notion that one mechanism contributing to EDC-based induction of epimutations
270 involves disruption of canonical endocrine signaling pathways. However, the fact that exposure to BPS
271 also induced epimutations in germ cells, even in the absence of expression of estrogen-related
272 receptors, and generated many DMCs in regions not inclusive of EREs, suggests that disruption of
273 canonical endocrine signaling pathways is not the only mechanism by which exposure to an EDC can
274 induce epimutations.

275 **Cell-type specific features of BPS-induced epimutations**

276 To further interrogate cell-type specific differences in the genesis of epimutations following
277 exposure to BPS, we compared DNA methylation patterns detected in the control (vehicle only) samples
278 to identify naturally occurring, cell-type specific DMCs inherently associated with each different cell fate.
279 Interestingly, of the 297,415 distinct CpGs interrogated by the Illumina Infinium Mouse Methylation
280 BeadChip Array used for this analysis, >240,000 showed some degree of inherent differential
281 methylation among the four cell types tested, suggesting they are tied to cell-fate specific differential
282 DNA methylation (Figure 4a). We next determined the extent to which DMCs induced specifically by
283 exposure of each cell type to BPS occurred at CpG dinucleotides that were among these naturally
284 occurring cell-type specific DMCs. We found that a large majority of BPS exposure-specific epimutations
285 detected in each cell type occurred at CpGs that also show inherent, cell-type specific variation in DNA
286 methylation (>95% of BPS-induced epimutations in somatic and pluripotent cell types and ~89% in germ
287 cells) (Figure 4a). As with the overall pattern of BPS-induced epimutations shown in Figure 2, BPS-
288 induced epimutations at CpGs showing inherent cell-type specific variation were enriched in apparent
289 enhancer regions that occurred near EREs in somatic and pluripotent cell types, whereas those in germ
290 cells were found predominantly in promoter regions containing significantly fewer EREs (Figure 4b,d).
291 However, the low percentage of BPS-induced epimutations that occurred at CpGs that did not show
292 inherent cell-type specific variation in DNA methylation patterns were found to be enriched in promoter

293 regions lacking nearby EREs in all four cell types (Figure 4c,d). Thus, this latter group of BPS-induced
294 epimutations appears to represent a small core group that arises following exposure to BPS via a
295 mechanism that does not rely upon disruption of canonical endocrine signaling, and so is common to all
296 cell types, regardless of expression of relevant endocrine receptors or nearby residence of relevant HREs
297 within the genome.

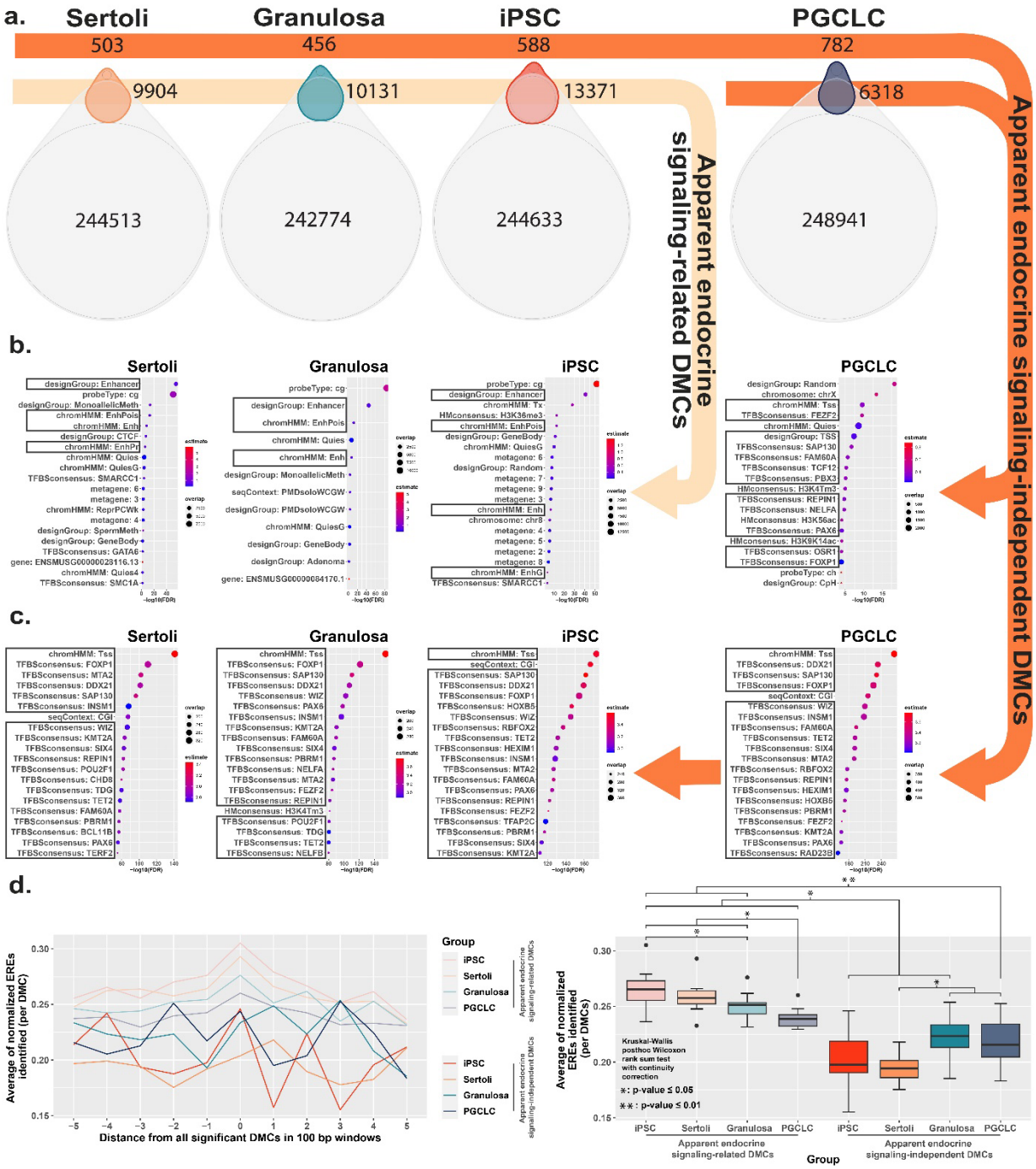

Figure 4. Direct comparison of BPS exposure-specific and cell-type specific features between cell types. a) Assessment Venn diagrams indicating DMCs that are due either to BPS exposure (top, smaller ovals) or inherent cell-type specific differences (bottom, larger ovals). Numbers of apparent endocrine-signaling related DMCs are shown in the light orange arrow, and apparent endocrine-signaling independent DMCs are shown in the dark orange arrows. Enrichment plots indicating feature annotations in genomic regions displaying **b)** apparent endocrine-signaling related DMCs occurring predominantly in enhancer regions in somatic Sertoli and granulosa cell types or pluripotent cells

306 expressing one or more estrogen receptors, or **c)** a smaller set of apparent endocrine-signaling
307 independent DMCs occurring predominantly in promoter regions in all four cell types regardless of +/-
308 expression of relevant endocrine receptors. **d)** Normalized density plots and box plots displaying the
309 frequency of ERE half-sites identified within 500 bp of apparent endocrine-signaling related DMCs
310 occurring predominantly in enhancer regions and apparent endocrine-signaling independent DMCs
311 occurring predominantly in promoters.

312

313 **Impact of BPS exposure on gene expression**

314 We next sought to determine if the cell-type specific differential susceptibility to BPS-induced
315 epimutagenesis translated to a similar extent of dysregulation of gene expression in each cell type. We
316 found that there was a similar relationship between the presence of DMCs in the promoter region of a
317 gene and differential expression of that gene in all four cell types examined (Supplement figure 2).
318 Somewhat surprisingly, RNA-seq analysis of gene expression patterns in each exposed cell type relative
319 to its corresponding control (same cell type exposed to carrier only) revealed the greatest number of
320 dysregulated genes in PGCLCs, despite PGCLCs being the cell type that showed the lowest number of
321 epimutations following exposure to BPS (Tables 1,2). iPSCs showed the second highest level of
322 dysregulated genes, while somatic Sertoli and granulosa cells showed relatively low levels of
323 dysregulated gene expression (Table 2). Indeed, numbers of dysregulated genes were three orders of
324 magnitude lower in differentiated somatic cells than in either pluripotent cells or germ cells (Table 2).

325 Because BPS-exposed PGCLCs showed the highest level of dysregulated genes, as well as the
326 highest enrichment of DMCs occurring primarily at promoters (Figure 2b), we next assessed the general
327 proximity between DMCs and promoter regions in each cell type to determine if DMCs in promoter
328 regions may be more likely to predispose dysregulated gene expression than DMCs elsewhere in the
329 genome (Figure 5a). Indeed, we found that in all four cell types, the smaller the median distance
330 between BPS-induced DMCs and neighboring promoter regions, the larger the number of BPS-induced
331 DEGs (Figure 5b). Thus, it appears that while PGCLCs showed the fewest overall BPS-induced DMCs

among the four cell types exposed to BPS, this exposure induced a higher proportion of epimutations in regions within or adjacent to promoters in this cell type. This, and the relatively high extent of decondensed chromatin genome-wide in fetal germ cells, appear to have contributed to the higher incidence of dysregulated gene expression in BPS-exposed PGCLCs than that observed in the other three BPS-exposed cell types, even though the overall numbers of BPS-induced epimutations were greater in the other cell types.

Table 2. Exposure-specific differentially expressed genes*

DEGs	Sertoli	Granulosa	iPSCs	PGCLCs
Down regulated	3	0	343	844
Up regulated	32	2	694	1,046
Total	35	2	1,037	1,890

*Genes showing significant differential expression following exposure of each cell type to 1µM BPS relative to matched control cell types exposed to carrier only.

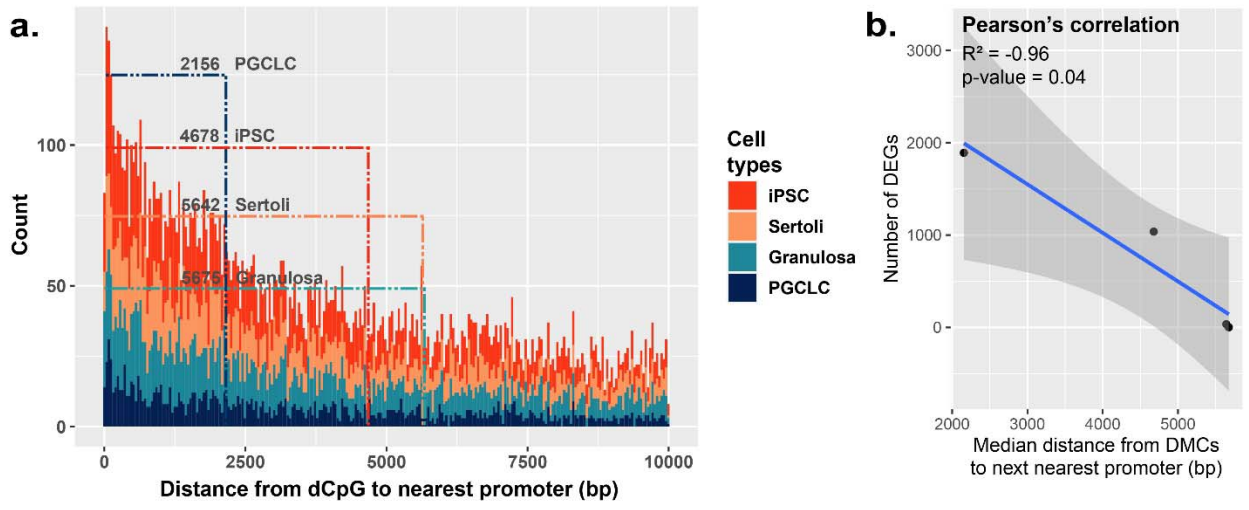

344 **Figure 5. Correlation between the proximity of DMCs to promoters and dysregulation of gene**
345 **expression. a)** Proximity plot displaying distances from exposure-specific DMCs to nearest promoter
346 regions. Dotted lines indicate median points of the data for each cell type. **b)** Correlation plot displaying
347 a negative relationship between the distance from DMCs to nearest promoters and resulting
348 dysregulation of gene expression within each cell type.

349

350 **Potential non-canonical signaling pathways disrupted by BPS exposure**

351 To identify potential mechanisms by which BPS exposure may induce epimutations via
352 disruption of non-canonical endocrine signaling pathways, we mined our RNA-seq data to identify genes
353 dysregulated independently of expression of relevant hormone receptors or presence of nearby EREs.
354 We identified a set of genes in all four cell types tested that displayed promoters enriched for apparent
355 endocrine-signaling independent DMCs (Supplement figure 7). Gene ontology (GO) analysis indicated
356 that several of the 1,957 genes we identified were associated with ubiquitin-like protease pathways,
357 including 124 of 800 genes that regulate protein degradation and 5 of 9 genes involving 1-
358 phosphatidylinositol-3 kinase activities, linked to the PI3K/AKT signaling pathway (Figure 6a).

359 Previous reports have established a link between ubiquitin-like protease pathways and classical
360 ER signaling (Beamish and Frick, 2022; Kabir et al., 2015), suggesting that genes related to ubiquitin-like
361 protease pathways that have promoters lacking EREs may be regulated by factors that are themselves
362 encoded by genes with promoters containing EREs, and so could be indirectly activated or repressed by
363 disruption of classical ER signaling. However, involvement of PI3K/AKT pathway signaling has previously
364 been linked to estrogen signaling through non-canonical G-protein coupled receptors such as GPER1,
365 which was sufficient to induce estrogen signaling in ER KO mouse cell lines which lack the capacity for
366 classical ER signaling (Filardo et al., 2002; Molina et al., 2017). To determine if our data support the
367 suggestion that the non-canonical BPS-induced changes were linked to involvement of PI3K/AKT
368 pathway genes, we performed GO analysis on the 1,890 DEGs identified in PGCLCs in which

369 epimutations appeared to be induced independent of classical ER signaling. Interestingly we detected no
370 apparent involvement of pathways involving ubiquitin-like proteases, but we did detect differential
371 expression of 4 of 7 genes associated with a pathway involving phosphatidylinositol-4 phosphatase
372 signaling which intersects with the PI3K/AKT signaling pathway (Figure 6b). Finally, while we did not
373 detect expression of *Gper1* transcripts, we did observe differential expression of genes encoding other
374 less well studied G-protein coupled receptors, including *Gprc5a*, *Gprc5b*, *Gpr89, Gpr107*, and *Gpr161* in
375 all four cell types exposed to BPS. These receptors have all been previously shown to bind either BPA or
376 17β-estradiol in rat models and could be potential targets of non-canonical BPS-induced estrogen
377 signaling (Figure 6c) as described in the following links:
378 (https://rgd.mcw.edu/rgdweb/report/gene/main.html?id=1305882,
379 https://rgd.mcw.edu/rgdweb/report/gene/main.html?id=1563245,
380 https://rgd.mcw.edu/rgdweb/report/gene/main.html?id=1304837,
381 https://rgd.mcw.edu/rgdweb/report/gene/main.html?id=1310804,
382 https://rgd.mcw.edu/rgdweb/report/gene/main.html?id=1309510)

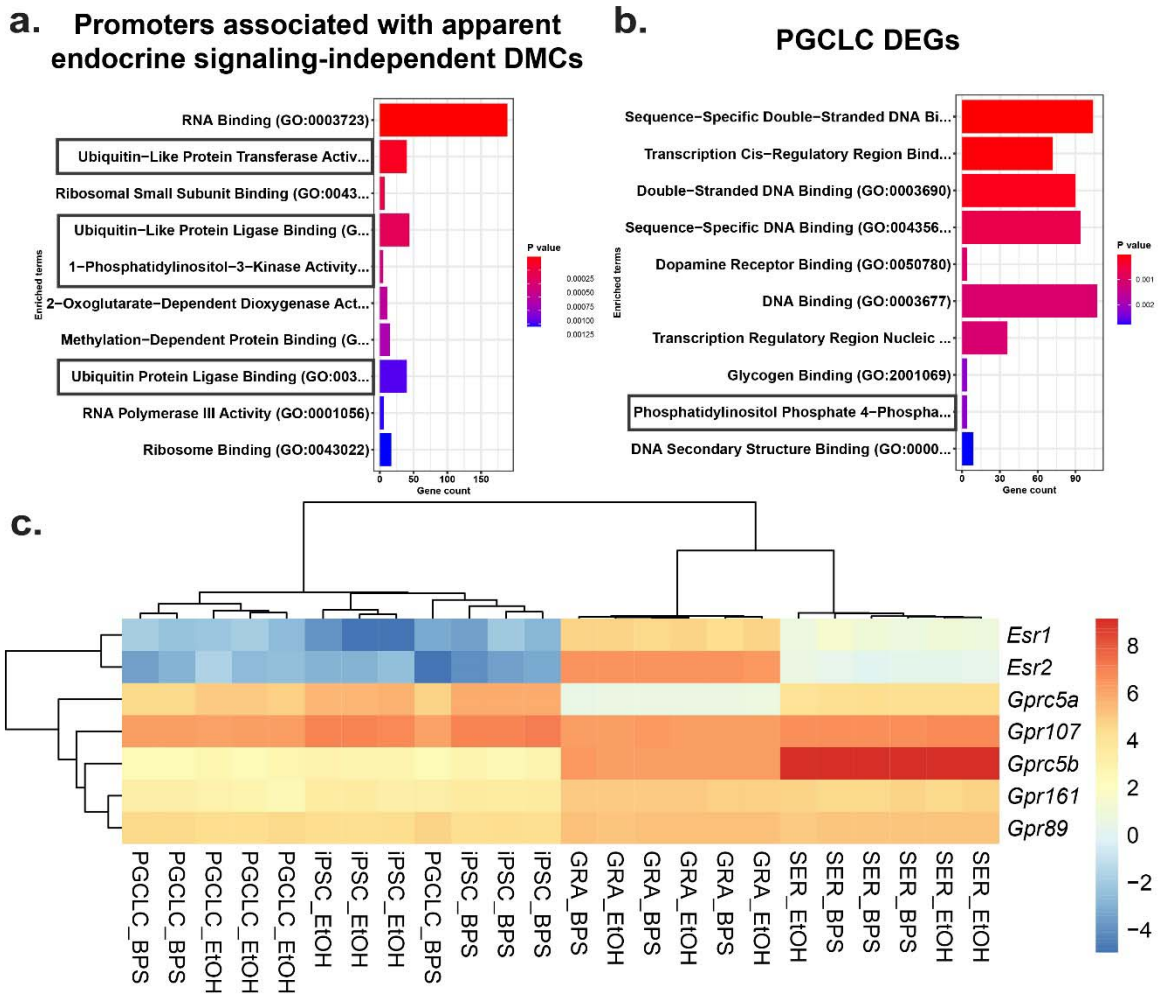

Figure 6. Potential involvement of non-canonical estrogen signaling pathways in BPS-induction of epimutations. Relative expression of genes **a)** enriched for apparent endocrine-signaling independent promoter-region DMCs found in all cell types or **b)** dysregulated in PGCLCs which lack expression of estrogen receptors. **c)** Heatmap of relative expression of estrogen receptor genes (*Esr1* and *Esr2*) and G-coupled protein receptors (*Gprc5a*, *Gpr107*, *Gprc5b*, *Gpr161*, and *Gpr89*) in pluripotent, somatic, and germ cell types. *Gprc5a*, *Gpr107*, *Gprc5b*, *Gpr161*, and *Gpr89* all have been shown to bind to BPA or 17β-estradiol in rat models and represent potential G-coupled protein receptors which could lead to the induction of endocrine-signaling independent DMCs.

Propagation of BPS-induced epimutations during transitions in cell fate

Transitions between pluripotent and germ cell fates, or vice versa, are accompanied by large-scale epigenetic reprogramming *in vivo* (Cantone and Fisher, 2013; Lee et al., 2014; Santos et al., 2002; Sanz et al., 2010), and these are recapitulated during similar transitions induced *in vitro* (Ishikura et al., 2016). To determine the extent to which BPS-induced epimutations persist during a pluripotent to

398 germline transition *in vitro*, we first exposed iPSCs to 1 μM BPS and then differentiated the exposed
399 iPSCs first into epiblast-like cells (EpiLCs) and then into PGCLCs, recapitulating the early germline
400 epigenetic reprogramming event that normally occurs *in vivo* (Kurimoto and Saitou, 2018; Ohta et al.,
401 2017) (Figure 7a). We then used genome-wide analyses by EM-seq and RNA-seq to compare numbers of
402 exposure-specific DMCs and DEGs, respectively, in PGCLCs derived from BPS-exposed iPSCs with those in
403 the directly exposed iPSCs and found lower, but still substantial numbers of both (28,168 vs 38,105
404 DMCs, and 1,437 vs 1,637 DEGs in the derived PGCLCs compared to the directly exposed iPSCs,
405 respectively) (Figure 7b,c).

406 When we compared the specific DMCs and DEGs that were detected in the BPS-exposed iPSCs
407 with those that were detected in the subsequently derived PGCLCs, we found that >90% of each were
408 not conserved during the pluripotent to germline transition in cell fate. Specifically, only 3.7% of the
409 DMCs and 8.4% of the DEGs detected in the BPS-exposed iPSCs were also detected in the PGCLCs
410 derived from the exposed iPSCs. Among the small portion of specific 138 DEGs that were conserved
411 from exposed iPSCs to derived PGCLCs, several (12.32%) (*Cdkn1a*, *Ccnd2*, *Plk2*, *Tgfbr1*, *Gadd45g*, *Lck*,
412 *Ltbr*, *Mad2l1*, *Ap3m2*, *Ctsz*, *Tcirg1*, *Gusb*, *Id2*, *Lefty2*, *Gstm7, Acsl1, Slc39a14*) were involved in cell cycle
413 and apoptosis pathways which could potentially be linked to cancer development (Supplement figure 8).
414 Thus, of the 38,105 DMCs and 1,637 DEGs induced by exposure of iPSCs to 1 μM BPS, 36,688 and 1,499,
415 respectively, did not persist during differentiation of iPSCs to form PGCLCs, and so were apparently
416 corrected by germline reprogramming. Simultaneously however, 26,752 novel DMCs and 1,299 novel
417 DEGs appeared in the derived PGCLCs that were not present in the BPS-exposed iPSCs, so were
418 apparently generated *de novo* during the germline reprogramming process. These results are consistent
419 with the notion that germline epigenetic reprogramming corrected many of the epimutations that were
420 present in the BPS-exposed pluripotent cells from which they were derived, but that exposure of cells to
421 EDCs may disrupt the underlying chromatin landscape in a way that then interferes with subsequent

422 reprogramming such that in addition to correcting many previously induced epimutations, the germline
423 reprogramming process, acting on a disrupted chromatin landscape, also generates many novel
424 epimutations *de novo* during the pluripotent to germline transition.

425 -

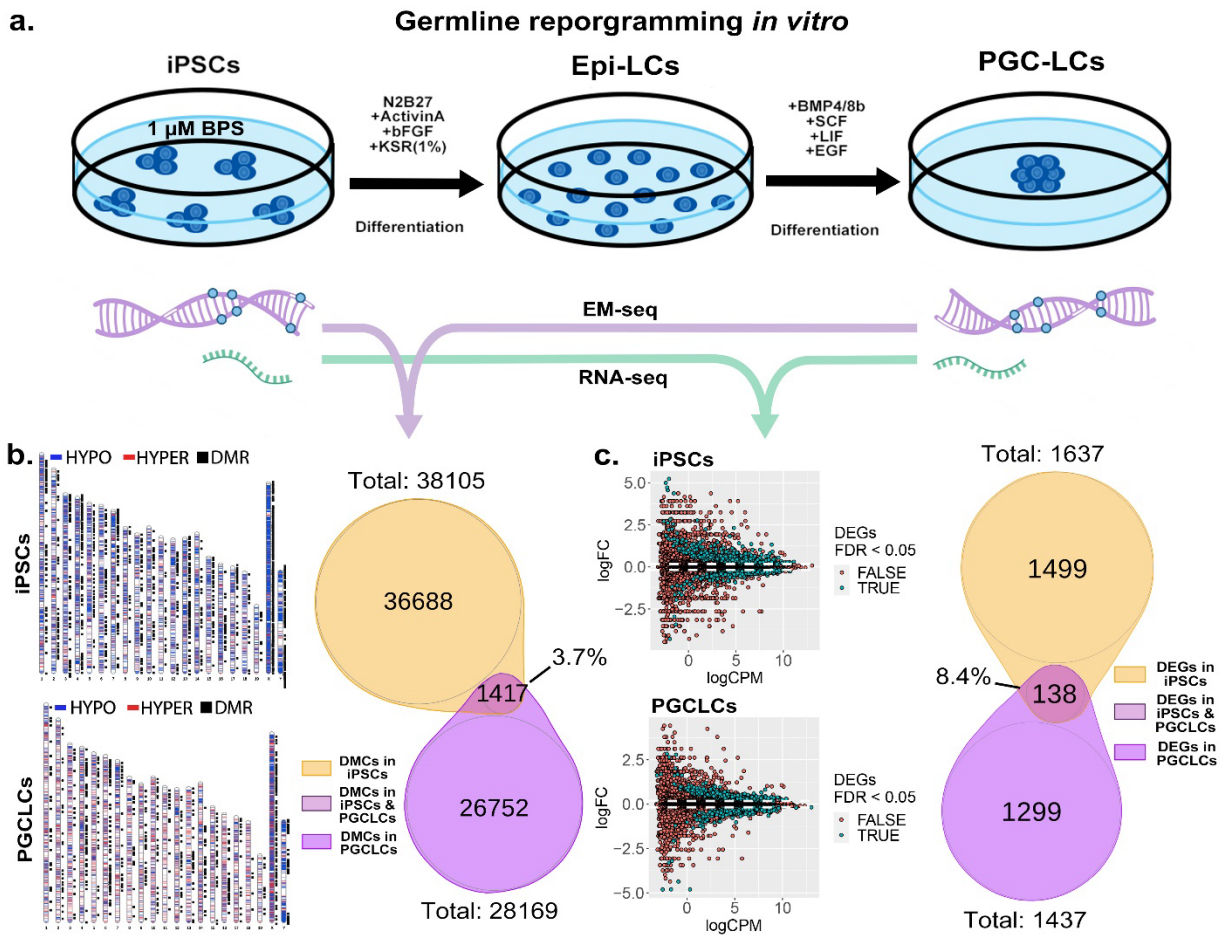

426

427 **Figure 7. Persistence of BPS-induced epimutations through recapitulation of early germline**
428 **reprogramming *in vitro*. a)** Schematic illustrating derivation of PGCLCs from iPSCs *in vitro*. iPSCs are first
429 induced to form EpiLCs which are then induced to form PGCLCs. iPSCs were exposed to either ethanol +
430 1 µM BPS or ethanol (carrier) only, then induced to undergo transitions to form EpiLCs and then PGCLCs.
431 **b)** DNA samples from BPS-exposed or control iPSCs as well as subsequently derived PGCLCs were
432 assessed for exposure-specific DNA methylation epimutations by EM-seq. BPS-treated iPSCs showed
433 38,105 DMCs and subsequently derived PGCLCs showed 28,169 DMCs. Of those, only 1,417 (3.7%) of the
434 DMCs were conserved from the BPS-exposed iPSCs to the subsequently derived PGCLCs. **c)** RNA samples
435 from BPS-exposed or control iPSCs and subsequently derived PGCLCs were assessed for global gene
436 expression patterns by RNA-seq. BPS-treated iPSCs showed 1,637 exposure-specific DEGs and
437 subsequently derived PGCLCs showed 1,437 exposure-specific DEGs. Of those, only 138 (8.4%) were
438 conserved from the BPS-exposed iPSCs to the subsequently derived PGCLCs.

439

440 **Discussion**

441 While nearly 20 years of research on the effects of exposure of live animals to various EDCs and
442 other environmental disruptive influences has clearly established the potential to perturb the
443 epigenome in ways that can dysregulate normal gene expression patterns and predispose the
444 development of disease states, the molecular mechanisms underlying these phenomena have remained
445 largely undefined. Thus, the manner in which environmental exposures introduce biochemical changes
446 in epigenetic programming, how such disruptions can be propagated within a tissue or throughout the
447 soma of an exposed individual or enter that individual's germ line, or how these disruptions predispose
448 disease states in that individual, or how a resulting prevalence of epimutations can be transmitted to
449 multiple subsequent generations despite generational epigenetic reprogramming, are all mechanistic
450 questions that have remained unanswered despite more than 5,000 publications on this topic since the
451 early 2000s. The vast majority of those publications have described experiments in animal models –
452 typically rodents. While informative, such live animal studies require months to years to complete, are
453 cost-, labor-, and animal-intensive, and have not yielded substantial insight into the molecular
454 mechanisms underlying the deleterious effects of environmentally-induced epimutations.

455 *In vitro* model systems have proven to be very useful tools for deciphering molecular
456 mechanisms related to normal development and homeostasis, or disruptions of those processes
457 predisposing onset of disease. Examples include cell culture systems used to study developmental
458 processes such as X-chromosome inactivation in mammals (Almeida et al., 2017; Patrat et al., 2009) or
459 early embryogenesis (Bao et al., 2022; Lau et al., 2022), or to elucidate the cellular and molecular
460 etiology of many different diseases based on the now popular "disease-in-a-dish" approach (Davaapil et
461 al., 2020; Song et al., 2023). While *in vitro* cell culture systems are, by nature, devoid of a majority of the
462 physiological complexities present within the intact organism *in vivo*, this provides an actual advantage

463 in that it facilitates deconvolution of those complexities while unequivocally focusing on only certain,
464 specific aspects or cell types. However, this ultimately warrants validation of results discerned from
465 studies of *in vitro* models to ensure they also reflect functions ongoing in the more complex and
466 heterogeneous environment of the intact animal *in vivo*.

467 We assembled an *in vitro* system in which we combined the three cell types normally involved in
468 i) the initial exposure to disruptive environmental effects (somatic cells), ii) the first phase of
469 generational epigenetic reprogramming in the preimplantation embryo (pluripotent cells), and iii) the
470 second phase of generational reprogramming in the developing germ line (germ cells). This system
471 allowed us to gain insights into multiple mechanistic aspects of environmentally-induced
472 epimutagenesis including the initial induction of epimutations by exposure of cells to the EDC, BPS, cell-
473 type specific differences in susceptibility to BPS-induced epimutagenesis, factors that appear to
474 contribute to that differential susceptibility, and the mechanism by which an epimutated state may
475 persist across multiple generations despite generational reprogramming.

476 Here we have shown that exposure of homogeneous populations of cells maintained in culture
477 to an EDC such as BPS can induce epimutagenesis and dysregulation of gene expression, and that this
478 occurs in a partially additive dose-dependent manner, although the quantitative effect appears to
479 plateau at higher doses. This afforded us the opportunity to test the relative effects of direct exposure
480 of different specific cell types to a similar dose of BPS with no confounding effects imposed by
481 interactions with other cell types or systemic effects of the sort that normally occur in the *in vivo*
482 context. We found that somatic, pluripotent, and germ cell types do indeed show differences in direct
483 susceptibility to induction of epimutations following exposure to BPS, both in terms of the quantity of
484 epimutations induced and qualities of the resulting epimutations such as a predominance of hyper-
485 versus hypomethylation, and the genomic locations where such epimutations tend to occur. Our results
486 suggest that these differences reflect distinctions in the normal status of each cell type at the time of

487 exposure. Thus, somatic, pluripotent, and germ cell types differ in the normal status of genome-wide
488 patterns of accessible versus inaccessible chromatin, global DNA methylation, and expression of relevant
489 endocrine receptors. Interestingly, our data suggest that all of these parameters can influence cell-type
490 specific susceptibility to induction of epimutations by exposure to BPS, and that different combinations
491 of these variables ultimately determine the quantity and quality of epimutations induced by exposure to
492 BPS. We note that while our exposure dose of 1 μM of BPS was below that deemed safe by the EPA for
493 exposure of humans to the similar EDC, BPA, that same dose may exert greater effects when used to
494 expose cells in culture in the absence of any sort of mitigating metabolic effects that may accrue in
495 intact animals or humans. Indeed, the potential to quantify the epimutagenic effects of different doses
496 of an EDC on different cell types as shown in our study could be used in future studies to assess the
497 relative effects of a specific dose of an EDC on a specific cell type when that cell type is exposed either in
498 a homogeneous culture or within an intact animal.

499 Endogenous fetal germline cells (e.g. PGCs and prospermatogonia in males) normally display
500 lower levels of global DNA methylation and higher levels of chromatin accessibility than pluripotent or
501 somatic cell types (Hajkova, 2011), yet PGCLCs developed fewer epimutations following exposure to BPS
502 than the other cell types. This appears to be explained by the fact that germline cells do not express
503 either estrogen receptor whereas pluripotent and somatic cell types express one or both of the two
504 estrogen receptors, apparently rendering them more susceptible to induction of epimutations following
505 exposure to the estrogen mimetic, BPS. This is consistent with the notion that EDCs impose disruptive
506 effects by interfering with canonical endocrine signaling pathways, and that notion is further supported
507 by our observation that, in the cell types that express one or both estrogen receptors, we observed a
508 prevalence of BPS-induced epimutations in genomic regions containing nearby EREs, whereas in PGCLCs,
509 which do not express either estrogen receptor, we did not observe a strong correlation between the
510 locations of BPS-induced epimutations and genomic EREs.

511 Nevertheless, we did observe induction of epimutations in PGCLCs exposed to BPS, suggesting
512 that while cell types expressing relevant endocrine receptors may display elevated susceptibility to EDC-
513 induced epimutagenesis presumably based on disruption of canonical endocrine signaling, this is not the
514 only mechanism by which EDCs can induce epimutations. Indeed, our results support the suggestion
515 that there may be at least two types of epimutations induced by exposure to EDCs – one that is
516 independent of canonical endocrine signaling and so occurs in all cell types regardless of expression of
517 relevant endocrine receptors or the genomic location of relevant HREs, and another that does involve
518 disruption of canonical endocrine signaling and so is elevated in cell types expressing relevant endocrine
519 receptors and predisposes the induction of epimutations in genomic regions near relevant HREs. Beyond
520 this, a comparison of the quantities of BPS-induced epimutations in pluripotent and somatic cell types,
521 which both express one or both estrogen receptors, but which differ with respect to elevated genome-
522 wide chromatin accessibility in pluripotent cells compared to much more limited chromatin accessibility
523 in somatic cell types (Cantone and Fisher, 2013; Santos et al., 2002), suggests that chromatin
524 accessibility also contributes to susceptibility to EDC-induced epimutagenesis.

525 One of our most intriguing findings was that, in addition to estrogen-receptor expressing
526 somatic and pluripotent cell types developing more epimutations than non-estrogen-receptor
527 expressing germ cells in response to exposure to BPS, the occurrence of epimutations in the former
528 (somatic and pluripotent) cell types was predominantly in enhancer regions whereas that in the latter
529 (germ) cell type was predominantly in gene promoters. As noted above, there was a significant increase
530 in the occurrence of BPS-induced epimutations near EREs in somatic and pluripotent cell types
531 compared to germ cells. A genome-wide analysis confirmed that ERE half-sites occur more frequently in
532 enhancer regions than in promoter regions (Supplement figure 5 and Supplement table 5) supporting
533 our suggestion that the higher prevalence of BPS-induced epimutations we observed in enhancer
534 regions in somatic and pluripotent cell types was due to disruption of canonical hormone signaling.

535 Our finding that PGCLCs, which do not express endocrine receptors, still accrued epimutations
536 following exposure to BPS indicates that in addition to inducing epimutations by disrupting canonical
537 endocrine signaling pathways, exposure to EDCs can induce epimutations via mechanisms that do not
538 involve disruption of such pathways. This notion is further supported by the occurrence of BPS-induced
539 epimutations in genomic regions that do not include nearby EREs, even though a prevalence of the
540 epimutations induced in PGCLCs were located in gene promoters. Pathway analysis of the genes in
541 which promoter-region epimutations were induced by exposure of PGCLCs to BPS suggests an apparent
542 endocrine-signaling independent group of genes that can become disrupted by exposure to an EDC via
543 non-canonical signaling which may occur through the PI3K/AKT pathway via G-protein coupled
544 receptors. While we observed expression of a number of G-protein coupled receptors known to bind to
545 either 17β-estradiol or BPA, further studies will be required to determine if any of these contribute to
546 susceptibility to BPS epimutagenesis.

547 As expected, disruption of normal epigenetic programming induced by exposure of cells to BPS
548 also led to dysregulation of gene expression. Thus, RNA-seq analysis detected differentially expressed
549 genes in all cell types exposed to BPS. Surprisingly, the greatest number of DEGs was detected in PGCLCs
550 which was the cell type that developed the lowest overall number of epimutations in response to
551 exposure to BPS. However, PGCLCs showed a higher prevalence of BPS-induced epimutations in gene
552 promoter regions than was observed in any of the other cell types, so it appears that promoter-region
553 epimutations impose the most direct impact on gene expression. As noted above, fetal germ cells
554 normally display the lowest level of global DNA methylation of any cell type at any developmental stage.
555 This is characteristic of the epigenetic ground state that accrues uniquely in developing germ cells
556 (Hajkova, 2011), and is believed to reflect a generally more accessible chromatin state genome-wide in
557 germ cells than in other cell types. Thus, it may be that the epigenetic ground state in developing germ

558 cells renders this cell type uniquely susceptible to epimutagenesis in gene promoter regions, thereby
559 predisposing a high level of dysregulation of gene expression in response to exposure to an EDC.

560 Finally, our *in vitro* system allowed us to follow the fate of BPS-induced epimutations through a
561 major transition in cell fate from pluripotent to germline cells during which a portion of the normal
562 generational germline epigenetic reprogramming process is known to occur (Kurimoto and Saitou,
563 2018). Thus, when we induced iPSCs previously exposed to 1 µM BPS to differentiate into PGCLCs, we
564 found that a substantial prevalence of epimutations persisted during this transition. However, very few
565 of the specific DMCs or the associated DEGs detected in the BPS-exposed iPSCs persisted in the
566 subsequently derived PGCLCs. Specifically, only 3.7 % of DMCs and 8.4 % of DEGs were conserved
567 between the BPS-exposed iPSCs and the subsequently derived PGCLCs. This suggests that exposure of
568 cells to EDCs has the potential to disrupt epigenetic programming in a way that then interferes with
569 subsequent generational reprogramming that normally accompanies either germline to pluripotent or
570 pluripotent to germline transitions in cell fate. Recent *in vivo* studies have suggested that exposure of
571 gestating female mice to the EDC tributyltin results in disruption not simply of the pattern of epigenetic
572 modifications but also of the underlying chromatin landscape (Chamorro-García et al., 2021; Chang et
573 al., 2022). In this context, our results are consistent with the suggestion that exposure of cells to EDCs
574 can disrupt the underlying chromatin landscape (e.g. the pattern of A and B chromatin compartments)
575 such that when the "normal" reprogramming machinery then acts on this disrupted landscape it
576 corrects many of the originally induced epimutations, but simultaneously induces many novel
577 epimutations *de novo*. This would predispose ongoing abnormalities in the underlying chromatin
578 landscape that would, in turn, lead to the recurring correction of many existing epimutations in concert
579 with the genesis of many novel epimutations during each subsequent generation.

580 We note that, with the exception of our analysis of granulosa cells, all of our studies were
581 carried out in "male" XY-bearing cells. It remains possible that XX-bearing cells might differ from XY-

582 bearing cells in the way(s) in which they respond to exposure to an EDC. However, the similarity we
583 observed between responses of XX granulosa cells and XY Sertoli cells suggest this may not be the case –
584 at least in cell types in which dosage compensation has been established by X-chromosome inactivation.

585 Taken together, our results demonstrate the utility of an *in vitro* cell culture approach for
586 pursuing molecular mechanisms underlying environmentally induced disruption of normal epigenetic
587 programming manifest as the formation of epimutations and dysregulated gene expression. This
588 approach clearly affords unique potential to reveal mechanisms responsible for the initial induction of
589 epimutations in response to direct exposure of cells to disruptive effects such as EDCs, as well as
590 offering potential means to elucidate mechanisms by which environmentally induced epimutations are
591 then propagated within the exposed individual and then to that individual's descendants. Knowledge of
592 these mechanisms will afford the best opportunity to understand how these defects may, in the future,
593 be better diagnosed, treated, and/or prevented. With the ever-expanding catalogue of potentially
594 hazardous man-made compounds permeating our environment, it is increasingly important that we
595 recognize the potential dangers such compounds may impose and maximize our ability to protect
596 ourselves from those dangers.

597

598 **Materials and methods**

599 **Key resources table**

Reagent type (species) or resource	**Designation**	**Source or reference**	**Identifiers**	**Additional information**
Genetic	$R26^{rtTA}$; $Col1a1^{2lox\text{-}4F2A}$	The Jackson	011011	

reagent (*M. musculus*)		Laboratory		
Cell line (*M. musculus*)	CF1 Mouse embryonic fibroblasts, MitC-treated	Thermo Fisher Scientific	A34959	
Chemical compound	Dulbecco's Modified Eagle Medium (DMEM)	Thermo Fisher Scientific	10313021	High glucose, pyruvate, no glutamine
Chemical compound	Fetal bovine serum (FBS)	Thermo Fisher Scientific	10439024	Embryonic stem-cell FBS, qualified, USDA-approved regions
Chemical compound	Leukemia inhibitory factor (LIF)	Millipore Sigma	ESG1107	ESGRO® Recombinant Mouse LIF Protein
Chemical compound	DMEM/F12	Thermo Fisher Scientific	21041025	No phenol red
Chemical compound	Insulin	Millipore Sigma	I1882	From bovine pancreas
Chemical compound	Apo-Transferrin	Millipore Sigma	T1147	From human
Chemical compound	Bovine Serum Albumin (BSA)	Thermo Fisher Scientific	15260037	Fraction V (7.5% solution)
Chemical compound	Progesterone	Millipore Sigma	P8783	
Chemical compound	Putrescine dihydrochloride	Millipore Sigma	P5780	
Chemical compound	Sodium selenite	Millipore Sigma	S5261	
Chemical compound	Neurobasal™	Thermo Fisher Scientific		No phenol red
Chemical compound	B-27™	Thermo Fisher Scientific	12587010	(50X), minus vitamin A
Chemical compound	Penicillin-streptomycin	Thermo Fisher Scientific	15070063	(5,000 U/mL)
Chemical compound	GlutaMAX™	Thermo Fisher Scientific	35050061	(100X)
Chemical compound	2-Mercaptoethanol	Thermo Fisher Scientific	21985023	(1000X)
Chemical compound	CHIR99021	BioVision	1677-5	
Chemical	PD0325901	Amsbio	04-0006-02	10 mM in DMSO

compound				
Chemical compound	Recombinant Human/Murine/Rat Activin A	PeproTech	120-14	Insect derived
Chemical compound	Recombinant Human FGF-Basic (FGF-2/bFGF)	Thermo Fisher Scientific	13256-029	
Chemical compound	KnockOut™ Serum	Thermo Fisher Scientific	10828028	
Chemical compound	Glasgow's MEM (GMEM)	Thermo Fisher Scientific	11710035	
Chemical compound	Recombinant human bone morphogenetic protein 4 (BMP-4)	R&D Systems	314-BP-010	
Chemical compound	Recombinant mouse stem cell factor (SCF)	R&D Systems	455-MC-010	
Chemical compound	Recombinant human epidermal growth factor (EGF), carrier free (CF)	R&D Systems	2028-EG-200	
Chemical compound	Dulbecco's phosphate-buffered saline (DPBS)	Thermo Fisher Scientific	14040133	
Chemical compound	Deoxyribonuclease I (DNaseI)	Millipore Sigma	DN25	From bovine pancreas
Chemical compound	Trypsin (2.5%)	Thermo Fisher Scientific	15090046	No phenol red
Chemical compound	Soybean trypsin inhibitor	Thermo Fisher Scientific	17075029	
Chemical compound	Collagenase type IV	Worthington	LS004188	From *Clostridium histolyticum*
Chemical compound	Sertoli Cell Medium	ScienCell Research Laboratories	4521	
Chemical compound	Ethanol (EtOH)	Fisher	BP28184	(200 Proof)
Chemical compound	BSA	Millipore Sigma	A9085	
Chemical compound	Heat inactivated (HI) FBS	Thermo Fisher Scientific	10082147	
Chemical compound	Trypsin-EDTA (0.25%)	Thermo Fisher	25200072	With phenol red

		Scientific		
Chemical compound	Bisphenol S (BPS)	Millipore Sigma	43034-100MG	
Chemical compound	Phenol:Chloroform:Isoamyl Alcohol (25:24:1, v/v)	Thermo Fisher Scientific	15593031	
Chemical compound	TRIzol™	Thermo Fisher Scientific	15596026	
Chemical compound	Isopropanol	Thermo Fisher Scientific	327272500	
Chemical compound	Proteinase K Solution (20 mg/mL)	Thermo Fisher Scientific	25530049	
Chemical compound	MaXtract High Density	Quiagen	129046	Phase lock gel tubes
Chemical compound	Sodium Acetate Solution	Thermo Fisher Scientific	R1181	3M, pH 5.2
Chemical compound	Glycogen (5 mg/ml)	Thermo Fisher Scientific	AM9510	
Chemical compound	NaCl	Thermo Fisher Scientific	J21618.36	
Chemical compound	Tris base	Millipore Sigma	77-86-1	
Chemical compound	Ethylenediaminetetra acetic acid (EDTA)	Millipore Sigma	E9884-100G	
Chemical compound	Sodium dodecyl sulfate (SDS)	Millipore Sigma	151-21-3	
Chemical compound	Triton X-100	Thermo Fisher Scientific	85111	
Chemical compound	RQ1 DNase	Promega	M6101	
Chemical compound	Propidium iodide	BioLegend	421301	FCy 5 µL/10^6 cells
Antibody	ERα	Thermo Fisher Scientific	MA1-310	Host: mouse, ICC 1:100
Antibody	ERβ	GeneTex	GTX70174	Host: mouse, ICC 1:100
Antibody	INHA	Invitrogen	PA5-13681	Host: rabbit, ICC 1:25
Antibody	FSHR	Affinity	AF5477	Host: rabbit,

				ICC 1:250
Antibody	SOX9	Abcam	ab185966	Host: rabbit, ICC 1:100
Antibody	GAPDH	Novus	NB300-221	Host: mouse, ICC 1:100
Antibody	WT1	Novus	NBP2-67587	Host: rabbit, ICC 1:100
Antibody	FUT4	GeneTex	GTX34467	Host: rabbit, ICC 1:50
Antibody	NANOG	Abcam	ab80892	Host: rabbit, ICC 1:100
Antibody	POU5F1	Abcam	ab19857	Host: rabbit, ICC 1:200
Antibody	SOX2	Abcam	ab97959	Host: rabbit, ICC 1:200
Antibody	ID4	Thermo Fisher Scientific	PA5-26976	Host: rabbit, ICC 1:50
Antibody	AR	Santa Cruz	sc-7305	Host: mouse ICC 1:50
Antibody	PPARγ	Santa Cruz	sc-7273	Host: mouse ICC 1:200
Antibody	RXRα	Invitrogen	433900	Host: mouse ICC 1:200
Antibody	PRDM1	Thermo Fisher Scientific	14-5963-82	Host: rat ICC 1:50
Antibody	Goat Anti Mouse Alexa 488	Abcam		Host: goat, ICC 1:1000
Antibody	Goat Anti Rabbit Alexa 647	Abcam	ab150199	Host: goat, ICC 1:200
Antibody	Goat Anti Rat Alexa 647	Thermo Fisher Scientific	A21247	Host: goat ICC 1:200
Antibody	FUT4 (IgM, κ), brilliant violet 421	BioLegend	125614	Host: mouse, FCy 5 µL/10^6 cells
Antibody	ITGB3 (IgG), PE	BioLegend	104307	Host: hamster, FCy 1 µL/10^6 cells
Antibody	IgM, κ Isotype control, brilliant violet 421	BioLegend	562704	Host: mouse, FCy 1.25 µL/10^6 cells
Antibody	IgG Isotype control, PE	BioLegend	400907	Host: hamster, FCy 1 µL/10^6 cells
Commercial assay or kit	RNA Clean & Concentrator-5	Zymo Research	R1016	
Commercial assay or kit	Genomic DNA Clean & Concentrator-10	Zymo Research	D4011	
Commercial	EZ DNA Methylation	Zymo	D5001	

assay or kit	Kit	Research		
Commercial assay or kit	SuperScript™ III One-Step RT-PCR System with Platinum™ Taq DNA Polymerase	Thermo Fisher Scientific	12574026	
Commercial assay or kit	PowerTrack™ SYBR Green Master Mix for qPCR	Thermo Fisher Scientific	A46109	
Commercial assay or kit	Infinium Mouse Methylation BeadChip	Illumina	20041558	
Commercial assay or kit	RNA ScreenTape & Reagents	Agilent	5067-5576	
Commercial assay or kit	DNA ScreenTape & Reagents	Agilent	5067-5583	
Commercial assay or kit	Qubit dsDNA (Broad Range) BR Assay Kit	Thermo Fisher Scientific	Q32850	
Commercial assay or kit	Qubit RNA (high sensitivity) HS Assay Kit	Thermo Fisher Scientific	Q32855	
Commercial assay or kit	NEBNext® Ultra™ II Directional RNA Library Prep Kit for Illumina®	New England BioLabs	E7765	
Commercial assay or kit	NEBNext® Poly(A) mRNA Magnetic Isolation Module	New England BioLabs	E3370	
Software, algorithm	ZEISS ZEN Microscopy Software	https://www.zeiss.com/microscopy/en/products/software/zeiss-zen.html	ZEN 3.7	
Software, algorithm	Primer-BLAST	https://www.ncbi.nlm.nih.gov/tools/primer-blast/		
Software, algorithm	QuantSudtio™ Design & Analysis Software	https://www.thermofisher.com/us/en/home/technical-resources/software-downloads/quantstudio-3-5-real-	QuantSudtio™ v1.5.1	

		time-pcr-systems.html		
Software, algorithm	Fiji	https://fiji.sc/	Fiji v1.54f	(Schindelin et al., 2012)
Software, algorithm	Bfastq2	https://support.illumina.com/downloads/bcl2fastq-conversion-software-v2-20.html	Bcl2fastq2 v2.20	
Software, algorithm	FastQC	https://www.bioinformatics.babraham.ac.uk/projects/fastqc/	FastQC 0.12.0	(Andrews et al., 2023; Smith and de Sena Brandine, 2021)
Software, algorithm	Wg-blimp	https://github.com/MarWoes/wg-blimp	Wg-blimp v0.10.0	(Lehle and McCarrey, 2023; Wöste et al., 2020)
Software, algorithm	R-Project for Statistical Computing	http://www.r-project.org/	R 4.2.1	Packages: Sesame (Ding et al., 2023; Triche et al., 2013; Zhou et al., 2022, 2018), stringr (Wickham and RStudio, 2022), kintr (Xie et al., 2023), SummarizedExperiment (Morgan et al., 2023), ggrepel (Slowikowski et al., 2023), pals (Wright, 2023), wheatmap (Zhou, 2022), tidyr (Wickham et al., 2023) magrittr (Bache et al., 2022), dplyr (Wickham et al., 2023), ggplot2 (Wickham et al., 2023), ggvenn (Yan, 2023), RColorBrewer (Neuwirth, 2022), RIdeogram (Hao et al.,

				2020), AnnotationDbi (Pagès et al., 2023), Mus.musculus (Team BC, 2015), BSgenome.Mmusculus.UCSC.mm10 (Team TBD, 2021), GenomicRanges (Lawrence et al., 2013), universalmotif (Tremblay, 2023), memes (Nystrom, 2023), Plyranges (Lee et al., 2019), rtracklayer (Lawrence et al., 2009), Rsubread (Liao et al., 2019), edgeR (Chen et al., 2016; McCarthy et al., 2012; Robinson et al., 2010)

Animal procedures

Mice were used as the primary source of cells for the establishment of cultures for the analysis of differential cell-type specific susceptibility to exposure to the EDC BPS at the cellular level. All mice were euthanized prior to dissection and isolation of the tissue or cell type to be used for experiments. All animals were bred on-site and maintained in one of the UTSA on-campus vivaria under controlled temperature and humidity conditions in a fixed 12-hour light, 12-hour dark cycle with free access to 5V5R extruded food and non-autoclaved convential RO water. 5V5R has been verified to contain a targeted level of 50 PPM total phytoestrogenic isoflavones (genistein, daidzein, and glycitein) and has been certified for use with estrogen-sensitive protocols limiting the effect of these plant-derived compounds. Euthanasia was performed by trained personnel using continuous CO_2 exposure at a rate of 3L/min until one minute after breathing had stopped. Euthanasia was confirmed by cervical dislocation. Tissue from euthanized mice was used to obtain somatic (Sertoli, granulosa, and mouse embryonic

613 fibroblast [MEF]) cells, and primordial germ cells [PGCs]. Both Sertoli and granulosa cells were isolated
614 from respective male and female mice euthanized at postnatal day 20 (P20). MEFs and PGCs were
615 isolated from fetuses at embryonic day 13.5 postcoitum (E13.5).

616 ***In vitro* generation and/or culture of pluripotent, somatic, and germ cells**

617 **Pluripotent cell culture**

618 Male mouse iPSCs were derived from a transgenic mouse line carrying the *tetO-4F2A* cassette
619 obtained from The Jackson Laboratories (011011) (The Jackson Laboratory, ME USA). iPSCs can be
620 induced from essentially any cell type carrying this reprogrammable cassette by exposure to Doxycycline
621 for one week as previously described (Carey et al., 2010; Hochedlinger et al., 2005). For this project,
622 iPSCs were reprogrammed from MEFs isolated from a single male (XY) E13.5 mouse fetus.
623 Reprogrammed colonies were picked and expanded via sub-passaging. Validation of reprogrammed
624 pluripotency was determined by positive immunocytochemical (ICC) staining for the pluripotent markers
625 POU5F1, SOX2, NANOG, and FUT4 (Supplement figure 10 and 12). Karyotyping was done on each
626 candidate iPSC line produced to confirm normal chromosome number and XY sex chromosome
627 constitution of each line prior to aliquots being prepared for long-term storage in liquid nitrogen
628 (Supplement figure 11). We selected a male (XY) iPSC line to be used for this project. Upon thawing,
629 iPSCs were initially maintained on CF-1 feeder cells for a minimum of three passages. Cells were cultured
630 in DMEM supplemented with 15% fetal bovine serum (FBS) and 1000 U/mL leukocyte inhibitory factor
631 (LIF). Once pluripotent cells were stabilized in culture, they were transitioned to feeder-free conditions
632 and were cultured in N2B27 media supplemented with 2i and LIF for two-three passages prior to use in
633 chemical exposure experiments. A complete list of the media components along with catalog numbers
634 can be found in Supplementary File 1b.

635 **Sertoli cell culture**

636 Primary cultures of Sertoli cells were established as previously described (Karl and Griswold,
637 1990). Briefly, whole testes were dissected from juvenile mice at P20. Following removal of the tunica
638 albuginea from each individual testis, the bundles of seminiferous tubules were physically chopped
639 using a sterile razor blade to break down the coiled structure of tubules increasing the surface area and
640 rendering them easier to digest. These shortened fragments of seminiferous tubules were then digested
641 in a mixture of 2.5% trypsin and 6.64 mg/ml DNaseI in DPBS for 25 minutes at 37°C. After these enzymes
642 were inactivated, the tubule sections were washed multiple times, then treated with a final enzymatic
643 mixture of collagenase IV (0.70 mg/mL) and DNaseI (6.64 mg/mL) for 10 minutes to permeabilize the
644 thick collagen layer on the exterior of the seminiferous tubules to allow the Sertoli cells to migrate out
645 away from the tubules in culture. After checking the digested tubules under a microscope to confirm the
646 collagen layer had been permeabilized, the digested tubules were spun down to wash away the
647 enzymes, and then resuspended in Sertoli cell media containing retinoic acid from ScienCell™ (4521)
648 (ScienCell™ Research Laboratories, CA USA). The digested tubules were plated into 6 culture flasks in
649 order to have 3 replicates of both control and treated cells for each exposure experiment. To remove
650 contaminating germ cells from this primary culture, the cells were treated with hypotonic shock
651 treatment on the morning of the second day of culture, and the enriched Sertoli cells were washed and
652 allowed to recover with fresh media for at least two hours. The enriched primary cultures of Sertoli cells
653 were then ready to be used for chemical exposure experiments. The estimated purity of the culture was
654 > 80% based on ICC staining for the Sertoli cell markers SOX9 and WT1 (Supplement figure 12). A full
655 procedure for the establishment of primary cultures of Sertoli cells can be found in Supplementary File
656 1d.

657 **Granulosa cell culture**

658 Primary cultures of granulosa cells were established by selecting early preantral primary follicles
659 from enzymatically digested ovary tissue as described previously (Monti and Redi, 2016; Roy and

660 Greenwald, 1996), followed by breaking selected primary follicles down into a single cell suspension that
661 could be plated and maintained. To isolate preantral primary follicles we dissected ovaries from female
662 mice at P20 and then enzymatically digested the ovary using collagenase IV (560 U/pair of ovaries) for
663 25 minutes at 37°C with constant agitation. This digestion was stopped by addition of buffer with 0.5%
664 BSA and the mixture was spun down at 60xg for 5 minutes to pellet the cells. The cells were
665 resuspended in PBS with 0.5% BSA and transferred to a sterile petri dish under a stereomicroscope.
666 Primary follicles were individually picked from the solution using a glass needle with suction control and
667 moved into a clean droplet of PBS containing 0.5% BSA. Selected primary follicles were then spun down
668 at 1000xg for 5 mins. After spinning, the supernatant was removed, and the cells were finger-vortexed
669 to resuspend the pellet. The follicles were then digested to single cell suspension by addition of pre-
670 warmed (37°C) 0.25% trypsin and incubated for 5 mins with regular pipetting followed by pelleting again
671 at 1000xg for 5 mins. The trypsin-containing supernatant was removed, and the granulosa cells were
672 resuspended in DMEM supplemented with 15% FBS and plated into 6 culture flasks in order to have 3
673 replicates of both control and treated cells for each exposure experiment. The oocytes were non-
674 adherent and were washed away on day 2 when changing the media. The estimated purity of the
675 culture was > 90% based on ICC staining for the granulosa cell marker FSHR and INHA (Supplement
676 figure 12). The granulosa cells were then ready to be used for EDC exposure experiments. A full
677 procedure for the establishment of primary cultures of granulosa cells can be found in Supplementary
678 File 1e.

679 **Primordial germ cell like cell culture**

680 Mouse iPSCs were differentiated into PGCLCs as previously described (Hayashi et al., 2011).
681 Briefly, iPSCs maintained in N2B27 supplemented with 2i and LIF under feeder-free conditions were
682 differentiated to EpiLCs for two days by the addition of activin A and basic fibroblast growth factor
683 (bFGF) to the N2B27 media. After two days the EpiLC intermediate cells were passaged to low

684 adherence round bottom plates for 4 days in GK15 media containing bone morphogenic protein 4
685 (BMP4), stem cell factor (SCF), epidermal growth factor (EGF), and LIF to induce the differentiation of a
686 subset of cells (2-3%) in the resulting aggregate to become PGCLCs. 6 batches each being made up of 6
687 plates were required in order to obtain sufficient cell numbers for 3 replicates of both control and
688 treated conditions. During this four-day period, cell aggregates were ready for EDC exposure (see
689 below). Following EDC exposure, cell aggregates were removed from the low adherence round bottom
690 plates within each batch, dissociated into a single cell suspension, and PGCLCs were fluorescence-
691 activated cell sorted (FACS) on a BD FACSAria™ II in the UTSA Cell Analysis Core to recover cells that
692 were double-positive for FUT4 and ITGB3. A full list of the media components and catalog numbers for
693 the differentiation of iPSCs to PGCLCs along with our FACS gating for double positive FUT/ITGB3 PGCLCs
694 can be found in Supplementary File 1b and Supplement figure 13, respectively. Additional data
695 demonstrating validation of PGCLCs by qRT-PCR and ICC staining are shown in Supplement figure 13.

696 **Immunocytochemistry (ICC)**

697 Cells were immunolabeled as previously described (Rodig, 2022) to validate the purity of cell
698 primary cultures using known cell specific markers (Supplement figure 12) to detect the presence or
699 absence of relevant endocrine receptors ERα and ERβ at the protein level. Pluripotent (iPS) and somatic
700 (Sertoli and granulosa) cells were grown on 13mm Thermanox® plastic coverslips (174950) prior to
701 fixation, permeabilization, and immunolabeling (Nalge Nunc International, NY USA). Non-adherent germ
702 (PGC and PGCLC) cells were spun down onto poly-L-lysine coated slides (63410-01) at 400 RPM for one
703 minute using a Thermo Shandon CytoSpin III Cytocentrifuge from Rakin (Electron Microscopy Sciences,
704 PA USA & Rakin Biomedical Corporation, MI USA). Cells were fixed with 4% formaldehyde for 10 mins at
705 room temp (RT) and then washed three times for five minutes each with ICC buffer (PBS containing
706 0.01% Triton X-100 detergent) to permeabilize the cell and nuclear membranes prior to blocking with 5%
707 goat serum which was added to the ICC buffer and incubated for one hour at RT. Following blocking,

708 primary antibodies, in ICC buffer, were added to the slides and left to incubate overnight at 4°C. The
709 following day, slides were washed three times with ICC buffer, and fluorescent secondary antibodies in
710 ICC buffer were then added to the slides and left to incubate in the dark for 1 hour. After secondary
711 antibody incubation, cellular nuclei were stained with DAPI at a 1:1000 dilution in ICC buffer for 7
712 minutes, followed by 3 final washes with ICC buffer for 5 minutes. Coverslips then were transferred to
713 microscope slides and mounted with 5-10 µL of VECTASHEILD Antifade Mounting Medium (H-1000) and
714 sealed with clear nail polish before being imaged on a Zeiss AXIO Imager.M1 Fluorescence Microscope
715 (Vector Laboratories Inc, CA USA & Zeiss Group, Oberkochen DE). Images were processed for contrast
716 and brightness enhancement and for the addition of scale bars using Fiji (Schindelin et al., 2012).
717 Information about the primary and secondary antibodies along with catalogue numbers and dilutions
718 used can be found in the Key resources table.

719 **Quantitative RT-PCR (qRT-PCR)**

720 Total RNA was extracted from 3 replicate preps of cells as described previously (Rio et al., 2010)
721 and treated with 1.5 U/µg total RNA RQ1 DNase1 (M6101) to remove contaminating genomic DNA
722 (Promega™ Corporation, WI USA). 50 ng of cleaned RNA was retrotranscribed with SuperScript™ III as
723 recommended by the manufacturer (Invitrogen, MA USA). Primers were designed using Primer-BLAST
724 (Ye et al., 2012) from NCBI. A complete list of all primer sequences used in this study can be found in
725 Supplement table 13. Relative expression levels of selected genes were assessed by real-time PCR using
726 the PowerTrack™ SYBR Green Master Mix according to the manufacturer's instructions (Applied
727 Biosystems, MA USA) then run on a QuantStudio™ 5 Real-Time PCR System (Thermo Fisher Scientific,
728 MA USA) and analyzed with QuantStudio™ Design & Analysis Software. Each sample was normalized
729 based on constitutive expression of the *Gusb* reference gene to obtain the ΔCt [(2-[Ctgene-CtGusb)].

730 **BPS exposure design**

731 Despite numerous studies illustrating the dangers of estrogenic mimetic EDCs, the EPA has
732 currently not published any limits concerning the maximum acceptable dose of BPS below which
733 exposure on a daily basis is considered to be safe. Thus for this study, we established our initial testing
734 range of 1 µM, 50 µM, and 100 µM of BPS based on the limit established for BPA at ≤ 4.44 µM (Ribeiro
735 et al., 2019) selecting 1 dose below the established safe limit and two doses that exceed that limit. For
736 all cell types except PGCLCs, BPS was added to media gassed with 5% CO_2, 5% O_2, and balanced N_2 and
737 then injected into 3 replicate sealed T-25 cell culture flasks and left to incubate for 24 hours
738 (Supplement figure 15). The media was gassed to ensure enrichment to 5% CO_2, which is normally
739 regulated by the cell incubator, limiting the potential for the pH to change in the media during this
740 exposure period due to the absorption of CO_2 by incubating cells. Following 24 hours of exposure, media
741 containing BPS was removed and cells were washed and allowed to recover in fresh untreated media
742 (without BPS or EtOH) for 24 hours prior to harvesting. PGCLCs were not suitable for this exposure
743 paradigm as EpiLCs undergo differentiation to PGCLCs in cell aggregates formed in low-adherence
744 round-bottom 96 well plates and cannot be maintained in T-25 sealed flasks. Therefore, diluted BPS was
745 added to PGCLC media and added to cells in 3 replicate batches of round-bottom 96 well plates to
746 incubate for 24 hours prior to a shortened wash and "chase" period of 8 hours prior to cell sorting.

747 **Methylation beadchip analysis**

748 A total of 1µg of extracted genomic DNA from each of 3 replicate exposure experiments for each
749 cell type was bisulfite-converted with the EZ DNA Methylation Kit (D5001) and modified according to the
750 manufacturer's recommendations (Zymo Research, CA USA & Illumina, CA USA). These samples were
751 run on the Infinium Mouse Methylation BeadChip Array following the Illumina Infinium HD Methylation
752 protocol. This beadchip array includes 297,415 cytosine positions within the mouse genome (CpG sites,
753 non-CpG sites, and random SNPs). The methylation score for each CpG is represented as a β-value which
754 is a ratio of the fluorescence intensity ranging between 0 (unmethylated) and 1 (methylated). Arrays

755 were scanned by HiScan (Illumina, CA USA). Quality control (Supplement figure 16) and downstream
756 data processing of the .idat files was using the Sensible Step-wise Analysis of DNA Methylation
757 BeadChips (SeSAMe) Bioconductor package (Ding et al., 2023; Triche et al., 2013; Zhou et al., 2022,
758 2018). DNA methylation levels of differentially methylated cytosines (DMCs) are determined using
759 mixed linear models. This general supervised learning framework identifies CpG loci whose differential
760 methylation is associated with known control vs. treated co-variates. CpG probes on the array were
761 defined as having differential changes that met both p-value and FDR ≤ 0.05 significant thresholds
762 between treatment and control samples for each cell type analyzed. Additionally, we followed up our
763 DNA methylation analysis of individual dCpGs by identifying differentially methylated regions (DMRs).
764 DMRs were created by grouping all CpGs measured on the array into clusters using Euclidean distance
765 (Ding et al., 2023; Triche et al., 2013; Zhou et al., 2022, 2018). The p-values from the differential
766 methylation of individual CpGs within the resulting CpG clusters were aggregated, and clusters were
767 then filtered selecting for regions that contained a p-value ≤ 0.05 (Ding et al., 2023; Triche et al., 2013;
768 Zhou et al., 2022, 2018).

769 **RNA-seq**

770 Total RNA was extracted from 3 replicate preps of cells using Trizol as previously described (Rio
771 et al., 2010). Contaminating genomic DNA was removed by RQ1 DNase (M6101) treatment according to
772 the manufacturer's instructions (Promega Corporation, WI USA). RNA concentration was determined
773 using Qubit (Q32855) and RNA integrity (RIN) scores were determined using tape station (5067-5576)
774 according to the manufacturer's instructions (Thermo Fisher Scientific Inc, MA USA & Agilent
775 Technologies, Inc CA USA). Strand-specific RNA-seq libraries were prepared with the NEBNext® Ultra™ II
776 Directional RNA Library Prep Kit for Illumina® sequencing (E7760S) according to the manufacturer's
777 protocol (New England Biolabs, MA USA). Briefly, this process consisted of poly(A) RNA selection, RNA
778 fragmentation, and double stranded cDNA generation using random oligo(dT) priming followed by end

779 repair to generate blunt ends, adaptor ligation, strand selection, and polymerase chain reaction
780 amplification to generate the final library. Distinct index adaptors were used for multiplexing samples
781 across multiple sequencing lanes. Sequencing was performed on an Illumina NovaSeq 6000 instrument
782 yielding sequences of paired end 2x50 base pair runs. Demultiplexing was performed with the Illumina
783 Bcl2fastq2 program (Illumina, CA USA).

784 **RNA-seq expression analysis**

785 The quality of the fastq reads was checked using FastQC (Andrews et al., 2023; Smith and de
786 Sena Brandine, 2021) (Supplement figure 17). Reads were aligned to the mm10 mouse reference
787 genome using the Rsubreads package to produce read counts (Liao et al., 2019). These were then used
788 for differential gene expression analysis using the edgeR package (Chen et al., 2016; McCarthy et al.,
789 2012; Robinson et al., 2010). Briefly, gene counts were normalized using the trimmed mean of M-value
790 normalization (TMM) method before determining counts per million (CPM) values (Robinson and
791 Oshlack, 2010). For a gene to be classified as showing differential gene expression between BPS-treated
792 and EtOH vehicle-only control samples, a threshold of both a Benjamini-Hochberg adjusted p-value ≤
793 0.05 and a false discovery rate (FDR) ≤ 0.05 had to be met.

794 **EM-Seq**

795 Genomic DNA was extracted from 3 replicates of cells as previously described (Sambrook and
796 Russell, 2006). Smaller fragmented DNA (≤ 10 kb) and contaminating RNA were removed by cleaning the
797 genomic DNA on a genomic DNA clean and concentrator™-10 column (D4011), according to the
798 manufacturer's instructions (Zymo Research, CA USA). DNA concentration was determined using a Qubit
799 (Q32850) and genomic DNA (100 ng) was sheered using a Bioruptor® and the size of the sheered DNA
800 was determined using a TapeStation 4200 according to the manufacturer's instructions in the UTSA
801 Genomics Core (Diagenode Inc, NJ USA & Agilent Technologies, Inc CA USA). Large size (470-520 bp) EM-

802 seq libraries were prepared with the NEBNext® Enzymatic Methyl-seq kit (E7120S) according to the
803 manufacturer's protocol (New England Biolabs, MA USA). Briefly, this process consisted of A-tailing,
804 adaptor ligation, DNA oxidation by TET2 initiated by the addition of Fe (II), strand denaturization with
805 formamide, deamination by APOBEC3A, polymerase chain reaction amplification, and bead selection to
806 generate the final libraries. Distinct index adaptors were used for multiplexing samples across multiple
807 sequencing lanes. Sequencing was performed on an Illumina NovaSeq 6000 instrument yielding
808 sequences of paired end 2x150 base pair runs. Demultiplexing was performed with the Illumina
809 Bcl2fastq2 program (Illumina, CA USA).

810 **EM-Seq analysis of genome-wide DNA methylation patterns**

811 EM-seq data was processed using the comprehensive wg-blimp v10.0.0 software pipeline (Lehle
812 and McCarrey, 2023; Wöste et al., 2020). In brief, reads were trimmed prior to initiating the wg-blimp
813 pipeline using Trim Galore (https://www.bioinformatics.babraham.ac.uk/projects/trim_galore/).
814 Sequenced reads were aligned to the mm10 genome using gemBS (King et al., 2020; Merkel et al., 2019;
815 Schilbert et al., 2020). The BAM files from alignment underwent a series of QC tests including read
816 quality scoring by FastQC (Andrews et al., 2023), overall and per-chromosome read coverage calculation,
817 GC content, duplication rate, clipping profiles by Qualimap (Okonechnikov et al., 2016), and
818 deduplication by the Picard toolkit (https://broadinstitute.github.io/picard/) (Supplement table 14).
819 Methylation calling was performed by MethylDackel (https://github.com/dpryan79/MethylDackel) and
820 statistically significant DMC/DMR calling was performed by the metilene (Jühling et al., 2016) and
821 BSmooth (Hansen et al., 2012) algorithms. Metilene uses a binary segmentation algorithm combined
822 with a two-dimensional statistical test that allows the detection of DMCs/DMRs in large methylation
823 experiments with multiple groups of samples. BSmooth uses a local-likelihood approach to estimate a
824 sample-specific methylation profile, then computes estimates of the mean differences and standard
825 errors for each CpG to form a statistic similar to that used in a t-test. Finally, potential regulatory regions

826 were identified through the use of MethylSeekR (Burger et al., 2013). Results from the pipeline were
827 displayed in the wg-blimp interactive results web browser that was built using the R Shiny local browser
828 hosting framework (Chang et al., 2023).

829

830 **Data availability**

831 Methylation beadchip, EM-seq, and RNA-seq data discussed in this publication have been uploaded and
832 can be obtained from the SRA BioProject PRJNA1026145 and GEO accession GSE252723.

833 **Article and author information**

834 **Author details**

835 1. **Jake D. Lehle**

836 • Department of Neuroscience, Developmental and Regenerative Biology, The University
837 of Texas at San Antonio, Texas, United States of America

838 **Contribution:** Conceptualization, Data curation, Software, Formal analysis, Validation,
839 Investigation, Visualization, Methodology, Writing – original draft

840 **Competing interests:** No competing interests declared

841 **ORCiD:** 0000-0002-0833-7068

842

843 2. **Yu-Huey Lin**

844 • Department of Neuroscience, Developmental and Regenerative Biology, The University
845 of Texas at San Antonio, Texas, United States of America

Contribution: Data curation, Formal analysis, Validation, Investigation, Visualization, Methodology

Competing interests: No competing interests declared

ORCiD: 0009-0003-1321-0680

3. **Amanda Gomez**
   - Department of Biomedical Engineering and Chemical Engineering, The University of Texas at San Antonio, Texas, United States of America

Contribution: Data curation, Software, Investigation, Visualization

Competing interests: No competing interests declared

ORCiD: 0000-0002-0767-1275

4. **Laura Chavez**
   - Department of Neuroscience, Developmental and Regenerative Biology, The University of Texas at San Antonio, Texas, United States of America

Contribution: Data curation, Investigation, Visualization

Competing interests: No competing interests declared

ORCiD: 0000-0001-6174-0430

5. **John R. McCarrey**

866 • Department of Neuroscience, Developmental and Regenerative Biology, The University
867 of Texas at San Antonio, Texas, United States of America

868 **Contribution:** Conceptualization, Supervision, Funding acquisition, Project administration

869 **For correspondence:** John.McCarrey@utsa.edu

870 **Competing interests:** No competing interests declared

871 **ORCiD:** 0000-0002-5784-9318

872

873 **Funding**

874 **National Institute of Health**
875 **NICHD P50 (HD98593)**

876 • John R. McCarrey

877 **National Institute of Health**
878 **NIDA (U01DA054179)**

879 • John R. McCarrey

880 **Robert J. and Helen C. Kleberg Foundation**

881 • John R. McCarrey

882 **Nancy Hurd Smith Foundation**

883 • John R. McCarrey

884

885 **Acknowledgments**

886 This work was supported by grants from the NIH to JRM (HD98593 and DA054179), and gifts from the
887 Robert J. Kleberg, Jr. and Helen C. Kleberg Foundation and the Nancy Hurd Smith Foundation. The
888 authors would like to thank: Michael Klein and the Genomics Core Facility and staff at the University of
889 Utah for their assistance with processing the Illumina Infinium Mouse Methylation Beadchip Array
890 samples; Sean Vargas at the UTSA Genomics Core for his expertise and supervision for utilizing
891 equipment to prepare sequencing libraries; Dr. Sandra Cardona at the UTSA Cell Analysis Core for her
892 expertise and supervision performing FACS to isolate cells; Dr. Brian Herman for use of his fluorescent
893 microscope for the collection of images; and Dr. Brian Bringham for biostatistics advice. This work
894 received computational support from UTSA's HPC cluster Arc, operated by Tech Solutions. Sequencing
895 data in this study was generated at the UT Health Genome Sequencing Facility, which is supported by UT
896 Health San Antonio, NIH-NCI P30 CA054174 (Cancer Center at UT Health San Antonio) and NIH Shared
897 Instrument grant S10OD030311 (S10 grant to NovaSeq 6000 System), and CPRIT Core Facility Award
898 (RP220662).

899

900 **Ethics**

901 All experimental procedures involving animals were approved in advance by the UTSA IACUC (Protocols
902 MU015 and MU016).

903

904

905

906

907 **References:**

908 Almeida M, Pintacuda G, Masui O, Koseki Y, Gdula M, Cerase A, Brown D, Mould A, Innocent C,
909 Nakayama M, Schermelleh L, Nesterova TB, Koseki H, Brockdorff N. 2017. PCGF3/5-PRC1 initiates
910 Polycomb recruitment in X chromosome inactivation. *Science (80-)* **356**:1081–1084.
911 doi:10.1126/science.aal2512

912 Andrews S, Krueger F, Segonds-Pichon A, Biggins L, Krueger C, Montgomery J. 2023. Babraham
913 Bioinformatics - FastQC A Quality Control tool for High Throughput Sequence Data.

914 Anway MD, Leathers C, Skinner MK. 2006. Endocrine disruptor vinclozolin induced epigenetic
915 transgenerational adult-onset disease. *Endocrinology* **147**:5515–5523. doi:10.1210/en.2006-0640

916 Bache S, Wickham H, Henry L, Rstudio. 2022. magrittr: A Forward-Pipe Operator for R.

917 Bao M, Cornwall-Scoones J, Sanchez-Vasquez E, Chen DY, De Jonghe J, Shadkhoo S, Hollfelder F,
918 Thomson M, Glover DM, Zernicka-Goetz M. 2022. Stem cell-derived synthetic embryos self-
919 assemble by exploiting cadherin codes and cortical tension. *Nat Cell Biol* **24**:1341–1349.
920 doi:10.1038/S41556-022-00984-Y

921 Beamish SB, Frick KM. 2022. A Putative Role for Ubiquitin-Proteasome Signaling in Estrogenic Memory
922 Regulation. *Front Behav Neurosci* **15**:807215. doi:10.3389/FNBEH.2021.807215/BIBTEX

923 Bourdeau V, Deschênes J, Métivier R, Nagai Y, Nguyen D, Bretschneider N, Gannon F, White JH, Mader S.
924 2004. Genome-Wide Identification of High-Affinity Estrogen Response Elements in Human and
925 Mouse. *Mol Endocrinol* **18**:1411–1427. doi:10.1210/ME.2003-0441

926 Brenker C, Rehfeld A, Schiffer C, Kierzek M, Kaupp UB, Skakkebæk NE, Strünker T. 2018. Synergistic
927 activation of CatSper Ca2+ channels in human sperm by oviductal ligands and endocrine disrupting
928 chemicals. *Hum Reprod* **33**:1915–1923. doi:10.1093/humrep/dey275

929 Burger L, Gaidatzis D, Schübeler D, Stadler MB. 2013. Identification of active regulatory regions from
930 DNA methylation data. *Nucleic Acids Res* **41**:e155–e155. doi:10.1093/NAR/GKT599

931 Cantone I, Fisher AG. 2013. Epigenetic programming and reprogramming during development. *Nat*
932 *Struct Mol Biol*. doi:10.1038/nsmb.2489

933 Carey BW, Markoulaki S, Beard C, Hanna J, Jaenisch R. 2010. Single-gene transgenic mouse strains for
934 reprogramming adult somatic cells. *Nat Methods* **7**:56–59. doi:10.1038/NMETH.1410

935 Chamorro-García R, Poupin N, Tremblay-Franco M, Canlet C, Egusquiza R, Gautier R, Jouanin I, Shoucri
936 BM, Blumberg B, Zalko D. 2021. Transgenerational metabolomic fingerprints in mice ancestrally
937 exposed to the obesogen TBT. *Environ Int* **157**. doi:10.1016/J.ENVINT.2021.106822

938 Chang RC, Egusquiza RJ, Huang Y, Amato AA, Joloya EM, Wheeler HB, Nguyen A, Shioda K, Odajima J,
939 Shioda T, Blumberg B. 2022. Heritable changes in chromatin contacts linked to transgenerational
940 obesity. *bioRxiv* 2022.10.27.514145. doi:10.1101/2022.10.27.514145

941 Chang W, Cheng J, Allaire J, Sievert C, Schloerke B, Xie Y, Allen J, McPherson J, Dipert A, Borges B,
942 Software P, PBC. 2023. shiny: Web Application Framework for R.

943 Chen Y, Lun ATL, Smyth GK, Burden CJ, Ryan DP, Khang TF, Lianoglou S. 2016. From reads to genes to
944 pathways: differential expression analysis of RNA-Seq experiments using Rsubread and the edgeR
945 quasi-likelihood pipeline. *F1000Research 2016 51438* **5**:1438. doi:10.12688/f1000research.8987.2

946 Davaapil H, Shetty DK, Sinha S. 2020. Aortic "Disease-in-a-Dish": Mechanistic Insights and Drug
947 Development Using iPSC-Based Disease Modeling. *Front Cell Dev Biol* **8**.
948 doi:10.3389/FCELL.2020.550504

949 Deb P, Bhan A, Hussain I, Ansari KI, Bobzean SA, Pandita TK, Perrotti LI, Mandal SS. 2016. Endocrine
950 disrupting chemical, bisphenol-A, induces breast cancer associated gene HOXB9 expression in vitro

951 and in vivo. *Gene* **590**:234–243. doi:10.1016/j.gene.2016.05.009

952 Diaz-Castillo C, Chamorro-Garcia R, Shioda T, Blumberg B. 2019. Transgenerational Self-Reconstruction
953 of Disrupted Chromatin Organization After Exposure To An Environmental Stressor in Mice. *Sci*
954 *Reports 2019 91* **9**:1–15. doi:10.1038/s41598-019-49440-2

955 Ding W, Kaur D, Horvath S, Zhou W. 2023. Comparative epigenome analysis using Infinium DNA
956 methylation BeadChips. *Brief Bioinform* **24**. doi:10.1093/BIB/BBAC617

957 Dunham I, Kundaje A, Aldred SF, Collins PJ, Davis CA, Doyle F, Epstein CB, Frietze S, Harrow J, Kaul R,
958 Khatun J, Lajoie BR, Landt SG, Lee BK, Pauli F, Rosenbloom KR, Sabo P, Safi A, Sanyal A, Shoresh N,
959 Simon JM, Song L, Trinklein ND, Altshuler RC, Birney E, Brown JB, Cheng C, Djebali S, Dong X, Ernst
960 J, Furey TS, Gerstein M, Giardine B, Greven M, Hardison RC, Harris RS, Herrero J, Hoffman MM, Iyer
961 S, Kellis M, Kheradpour P, Lassmann T, Li Q, Lin X, Marinov GK, Merkel A, Mortazavi A, Parker SCJ,
962 Reddy TE, Rozowsky J, Schlesinger F, Thurman RE, Wang J, Ward LD, Whitfield TW, Wilder SP, Wu
963 W, Xi HS, Yip KY, Zhuang J, Bernstein BE, Green ED, Gunter C, Snyder M, Pazin MJ, Lowdon RF,
964 Dillon LAL, Adams LB, Kelly CJ, Zhang J, Wexler JR, Good PJ, Feingold EA, Crawford GE, Dekker J,
965 Elnitski L, Farnham PJ, Giddings MC, Gingeras TR, Guigó R, Hubbard TJ, Kent WJ, Lieb JD, Margulies
966 EH, Myers RM, Stamatoyannopoulos JA, Tenenbaum SA, Weng Z, White KP, Wold B, Yu Y, Wrobel J,
967 Risk BA, Gunawardena HP, Kuiper HC, Maier CW, Xie L, Chen X, Mikkelsen TS, Gillespie S, Goren A,
968 Ram O, Zhang X, Wang L, Issner R, Coyne MJ, Durham T, Ku M, Truong T, Eaton ML, Dobin A, Tanzer
969 A, Lagarde J, Lin W, Xue C, Williams BA, Zaleski C, Röder M, Kokocinski F, Abdelhamid RF, Alioto T,
970 Antoshechkin I, Baer MT, Batut P, Bell I, Bell K, Chakrabortty S, Chrast J, Curado J, Derrien T,
971 Drenkow J, Dumais E, Dumais J, Duttagupta R, Fastuca M, Fejes-Toth K, Ferreira P, Foissac S,
972 Fullwood MJ, Gao H, Gonzalez D, Gordon A, Howald C, Jha S, Johnson R, Kapranov P, King B,
973 Kingswood C, Li G, Luo OJ, Park E, Preall JB, Presaud K, Ribeca P, Robyr D, Ruan X, Sammeth M,

974 Sandhu KS, Schaeffer L, See LH, Shahab A, Skancke J, Suzuki AM, Takahashi H, Tilgner H, Trout D,
975 Walters N, Wang H, Hayashizaki Y, Reymond A, Antonarakis SE, Hannon GJ, Ruan Y, Carninci P,
976 Sloan CA, Learned K, Malladi VS, Wong MC, Barber GP, Cline MS, Dreszer TR, Heitner SG, Karolchik
977 D, Kirkup VM, Meyer LR, Long JC, Maddren M, Raney BJ, Grasfeder LL, Giresi PG, Battenhouse A,
978 Sheffield NC, Showers KA, London D, Bhinge AA, Shestak C, Schaner MR, Kim SK, Zhang ZZ,
979 Mieczkowski PA, Mieczkowska JO, Liu Z, McDaniell RM, Ni Y, Rashid NU, Kim MJ, Adar S, Zhang
980 Zhancheng, Wang T, Winter D, Keefe D, Iyer VR, Zheng M, Wang P, Gertz J, Vielmetter J, Partridge
981 EC, Varley KE, Gasper C, Bansal A, Pepke S, Jain P, Amrhein H, Bowling KM, Anaya M, Cross MK,
982 Muratet MA, Newberry KM, McCue K, Nesmith AS, Fisher-Aylor KI, Pusey B, DeSalvo G, Parker SL,
983 Balasubramanian Sreeram, Davis NS, Meadows SK, Eggleston T, Newberry JS, Levy SE, Absher DM,
984 Wong WH, Blow MJ, Visel A, Pennachio LA, Petrykowska HM, Abyzov A, Aken B, Barrell D, Barson
985 G, Berry A, Bignell A, Boychenko V, Bussotti G, Davidson C, Despacio-Reyes G, Diekhans M, Ezkurdia
986 I, Frankish A, Gilbert J, Gonzalez JM, Griffiths E, Harte R, Hendrix DA, Hunt T, Jungreis I, Kay M,
987 Khurana E, Leng J, Lin MF, Loveland J, Lu Z, Manthravadi D, Mariotti M, Mudge J, Mukherjee G,
988 Notredame C, Pei B, Rodriguez JM, Saunders G, Sboner A, Searle S, Sisu C, Snow C, Steward C,
989 Tapanari E, Tress ML, Van Baren MJ, Washietl S, Wilming L, Zadissa A, Zhang Zhengdong, Brent M,
990 Haussler D, Valencia A, Addleman N, Alexander RP, Auerbach RK, Balasubramanian Suganthi,
991 Bettinger K, Bhardwaj N, Boyle AP, Cao AR, Cayting P, Charos A, Cheng Y, Eastman C, Euskirchen G,
992 Fleming JD, Grubert F, Habegger L, Hariharan M, Harmanci A, Iyengar S, Jin VX, Karczewski KJ,
993 Kasowski M, Lacroute P, Lam H, Lamarre-Vincent N, Lian J, Lindahl-Allen M, Min R, Miotto B,
994 Monahan H, Moqtaderi Z, Mu XJ, O'Geen H, Ouyang Z, Patacsil D, Raha D, Ramirez L, Reed B, Shi M,
995 Slifer T, Witt H, Wu L, Xu X, Yan KK, Yang X, Struhl K, Weissman SM, Penalva LO, Karmakar S,
996 Bhanvadia RR, Choudhury A, Domanus M, Ma L, Moran J, Victorsen A, Auer T, Centanin L,
997 Eichenlaub M, Gruhl F, Heermann S, Hoeckendorf B, Inoue D, Kellner T, Kirchmaier S, Mueller C,

998 Reinhardt R, Schertel L, Schneider S, Sinn R, Wittbrodt B, Wittbrodt J, Jain G, Balasundaram G,
999 Bates DL, Byron R, Canfield TK, Diegel MJ, Dunn D, Ebersol AK, Frum T, Garg K, Gist E, Hansen RS,
1000 Boatman L, Haugen E, Humbert R, Johnson AK, Johnson EM, Kutyavin T V., Lee K, Lotakis D,
1001 Maurano MT, Neph SJ, Neri F V., Nguyen ED, Qu H, Reynolds AP, Roach V, Rynes E, Sanchez ME,
1002 Sandstrom RS, Shafer AO, Stergachis AB, Thomas S, Vernot B, Vierstra J, Vong S, Wang Hao,
1003 Weaver MA, Yan Y, Zhang M, Akey JM, Bender M, Dorschner MO, Groudine M, MacCoss MJ, Navas
1004 P, Stamatoyannopoulos G, Beal K, Brazma A, Flicek P, Johnson N, Lukk M, Luscombe NM, Sobral D,
1005 Vaquerizas JM, Batzoglou S, Sidow A, Hussami N, Kyriazopoulou-Panagiotopoulou S, Libbrecht MW,
1006 Schaub MA, Miller W, Bickel PJ, Banfai B, Boley NP, Huang H, Li JJ, Noble WS, Bilmes JA, Buske OJ,
1007 Sahu AD, Kharchenko P V., Park PJ, Baker D, Taylor J, Lochovsky L. 2012. An integrated
1008 encyclopedia of DNA elements in the human genome. *Nature* **489**:57–74.
1009 doi:10.1038/NATURE11247

1010 Filardo EJ, Quinn JA, Raymond Frackelton A, Bland KI. 2002. Estrogen action via the G protein-coupled
1011 receptor, GPR30: stimulation of adenylyl cyclase and cAMP-mediated attenuation of the epidermal
1012 growth factor receptor-to-MAPK signaling axis. *Mol Endocrinol* **16**:70–84.
1013 doi:10.1210/MEND.16.1.0758

1014 Gassner FX, Reifenstein ECJ, Algeo JW, Mattox WE. 1958. Effects of hormones on growth, fattening, and
1015 meat production potential of livestock - PubMed. *Recent Prog Horm Res* **14**:183–210; discussion
1016 210-7.

1017 Goodman M, Mandel JS, Desesso JM, Scialli AR. 2014. Atrazine and pregnancy outcomes: A systematic
1018 review of epidemiologic evidence. *Birth Defects Res Part B - Dev Reprod Toxicol*.
1019 doi:10.1002/bdrb.21101

1020 Gpr107 (G protein-coupled receptor 107) - Rat Genome Database. n.d.

1021 https://rgd.mcw.edu/rgdweb/report/gene/main.html?id=1305882

1022 Gpr161 (G protein-coupled receptor 161) - Rat Genome Database. n.d.

1023 https://rgd.mcw.edu/rgdweb/report/gene/main.html?id=1563245

1024 Gpr89b (G protein-coupled receptor 89B) - Rat Genome Database. n.d.

1025 https://rgd.mcw.edu/rgdweb/report/gene/main.html?id=1304837

1026 Gprc5a (G protein-coupled receptor, class C, group 5, member A) - Rat Genome Database. n.d.

1027 https://rgd.mcw.edu/rgdweb/report/gene/main.html?id=1310804

1028 Gprc5b (G protein-coupled receptor, class C, group 5, member B) - Rat Genome Database. n.d.

1029 https://rgd.mcw.edu/rgdweb/report/gene/main.html?id=1309510

1030 Guerrero-Bosagna C, Covert TR, Haque MM, Settles M, Nilsson EE, Anway MD, Skinner MK. 2012.

1031 Epigenetic transgenerational inheritance of vinclozolin induced mouse adult onset disease and

1032 associated sperm epigenome biomarkers. *Reprod Toxicol* **34**:694–707.

1033 doi:10.1016/j.reprotox.2012.09.005

1034 Hajkova P. 2011. Epigenetic reprogramming in the germline: Towards the ground state of the

1035 epigenome. *Philos Trans R Soc B Biol Sci*. doi:10.1098/rstb.2011.0042

1036 Hansen KD, Langmead B, Irizarry RA. 2012. BSmooth: from whole genome bisulfite sequencing reads to

1037 differentially methylated regions. doi:10.1186/gb-2012-13-10-R83

1038 Hao Z, Lv D, Ge Y, Shi J, Dolf W, Yu G, Chen J. 2020. RIdeogram: Drawing SVG Graphics to Visualize and

1039 Map Genome-Wide Data on Idiograms.

1040 Hayashi K, Ohta H, Kurimoto K, Aramaki S, Saitou M. 2011. Reconstitution of the mouse germ cell

1041 specification pathway in culture by pluripotent stem cells. *Cell* **146**:519–532.

1042 doi:10.1016/j.cell.2011.06.052

1043 Henley D V, Korach KS. 2010. Physiological effects and mechanisms of action of endocrine disrupting
1044 chemicals that alter estrogen signaling. *Hormones* **9**:191–205. doi:10.14310/horm.2002.1270

1045 Hochedlinger K, Yamada Y, Beard C, Jaenisch R. 2005. Ectopic Expression of Oct-4 Blocks Progenitor-Cell
1046 Differentiation and Causes Dysplasia in Epithelial Tissues. *Cell* **121**:465–477.
1047 doi:10.1016/J.CELL.2005.02.018

1048 Huang W, Zhao C, Zhong H, Zhang S, Xia Y, Cai Z. 2019. Bisphenol S induced epigenetic and
1049 transcriptional changes in human breast cancer cell line MCF-7. *Environ Pollut* **246**:697–703.
1050 doi:10.1016/j.envpol.2018.12.084

1051 Ishikura Y, Yabuta Y, Ohta H, Hayashi K, Nakamura T, Okamoto I, Yamamoto T, Kurimoto K, Shirane K,
1052 Sasaki H, Saitou M. 2016. In Vitro Derivation and Propagation of Spermatogonial Stem Cell Activity
1053 from Mouse Pluripotent Stem Cells. *Cell Rep* **17**:2789–2804.

1054 Jühling F, Kretzmer H, Bernhart SH, Otto C, Stadler PF, Hoffmann S. 2016. metilene: fast and sensitive
1055 calling of differentially methylated regions from bisulfite sequencing data. *Genome Res* **26**:256.
1056 doi:10.1101/GR.196394.115

1057 Kabir ER, Rahman MS, Rahman I. 2015. A review on endocrine disruptors and their possible impacts on
1058 human health. *Environ Toxicol Pharmacol*. doi:10.1016/j.etap.2015.06.009

1059 Karaman EF, Ozden S. 2019. Alterations in global DNA methylation and metabolism-related genes
1060 caused by zearalenone in MCF7 and MCF10F cells. *Mycotoxin Res* **35**:309–20. doi:10.1007/s12550-
1061 019-00358-8

1062 Karl AF, Griswold MD. 1990. Sertoli cells of the testis: preparation of cell cultures and effects of
1063 retinoids. *Methods Enzymol* **190**:71–75. doi:10.1016/0076-6879(90)90010-X

1064 Kelce, William R, Stone, Christy R, Laws, Susan C, Gray, Earl. 1995. Persistent DDT metabolite p,p'-DDE is
1065 a potent androgen receptor antagonist. *Nature* **375**:6532–581.

1066 King DJ, Freimanis G, Lasecka-Dykes L, Asfor A, Ribeca P, Waters R, King DP, Laing E. 2020. A Systematic
1067 Evaluation of High-Throughput Sequencing Approaches to Identify Low-Frequency Single
1068 Nucleotide Variants in Viral Populations. *Viruses* **12**. doi:10.3390/V12101187

1069 Kurimoto K, Saitou M. 2018. Epigenome regulation during germ cell specification and development from
1070 pluripotent stem cells. *Curr Opin Genet Dev* **52**:57–64. doi:10.1016/J.GDE.2018.06.004

1071 Lau KYC, Rubinstein H, Gantner CW, Hadas R, Amadei G, Stelzer Y, Zernicka-Goetz M. 2022. Mouse
1072 embryo model derived exclusively from embryonic stem cells undergoes neurulation and heart
1073 development. *Cell Stem Cell* **29**:1445-1458.e8. doi:10.1016/J.STEM.2022.08.013

1074 Lawrence M, Gentleman R, Carey V. 2009. rtracklayer: an R package for interfacing with genome
1075 browsers. *Bioinformatics* **25**:1841–1842. doi:10.1093/BIOINFORMATICS/BTP328

1076 Lawrence M, Huber W, Pagès H, Aboyoun P, Carlson M, Gentleman R, Morgan MT, Carey VJ. 2013.
1077 Software for Computing and Annotating Genomic Ranges. *PLOS Comput Biol* **9**:e1003118.
1078 doi:10.1371/JOURNAL.PCBI.1003118

1079 Lee HJ, Hore TA, Reik W. 2014. Reprogramming the methylome: erasing memory and creating diversity.
1080 *Cell Stem Cell* **14**:710–9. doi:10.1016/j.stem.2014.05.008

1081 Lee S, Cook D, Lawrence M. 2019. Plyranges: A grammar of genomic data transformation. *Genome Biol*
1082 **20**:1–10. doi:10.1186/S13059-018-1597-8/FIGURES/5

1083 Lehle JD, McCarrey JR. 2023. Accelerating the alignment processing speed of the comprehensive end-to-
1084 end whole-genome bisulfite sequencing pipeline, wg-blimp. *Biol Methods Protoc* **8**.
1085 doi:10.1093/BIOMETHODS/BPAD012

1086 Liao Y, Smyth GK, Shi W. 2019. The R package Rsubread is easier, faster, cheaper and better for
1087 alignment and quantification of RNA sequencing reads. *Nucleic Acids Res* **47**.
1088 doi:10.1093/NAR/GKZ114

1089 Mason CE, Shu FJ, Wang C, Session RM, Kallen RG, Sidell N, Yu T, Liu MH, Cheung E, Kallen CB. 2010.
1090 Location analysis for the estrogen receptor-α reveals binding to diverse ERE sequences and
1091 widespread binding within repetitive DNA elements. *Nucleic Acids Res* **38**:2355.
1092 doi:10.1093/NAR/GKP1188

1093 McCarthy DJ, Chen Y, Smyth GK. 2012. Differential expression analysis of multifactor RNA-Seq
1094 experiments with respect to biological variation. *Nucleic Acids Res* **40**:4288–4297.
1095 doi:10.1093/NAR/GKS042

1096 Meccariello R, Chianese R, Chioccarelli T, Ciaramella V, Fasano S, Pierantoni R, Cobellis G. 2014. Intra-
1097 testicular signals regulate germ cell progression and production of qualitatively mature
1098 spermatozoa in vertebrates. *Front Endocrinol (Lausanne)*. doi:10.3389/fendo.2014.00069

1099 Merkel A, Fernández-Callejo M, Casals E, Marco-Sola S, Schuyler R, Gut IG, Heath SC. 2019. gemBS: high
1100 throughput processing for DNA methylation data from bisulfite sequencing. *Bioinformatics* **35**:737–
1101 742. doi:10.1093/BIOINFORMATICS/BTY690

1102 Molina L, Figueroa CD, Bhoola KD, Ehrenfeld P. 2017. GPER-1/GPR30 a novel estrogen receptor sited in
1103 the cell membrane: therapeutic coupling to breast cancer. *Expert Opin Ther Targets* **21**:755–766.
1104 doi:10.1080/14728222.2017.1350264

1105 Monti M, Redi CA. 2016. Isolation and Characterization of Mouse Antral Oocytes Based on Nucleolar
1106 Chromatin Organization. *J Vis Exp* **2016**. doi:10.3791/53616

1107 Morgan M, Obenchain V, Hester J, Pagès H. 2023. SummarizedExperiment container.

1108 Myers RM, Stamatoyannopoulos J, Snyder M, Dunham I, Hardison RC, Bernstein BE, Gingeras TR, Kent
1109 WJ, Birney E, Wold B, Crawford GE, Epstein CB, Shoresh N, Ernst J, Mikkelsen TS, Kheradpour P,
1110 Zhang X, Wang L, Issner R, Coyne MJ, Durham T, Ku M, Truong T, Ward LD, Altshuler RC, Lin MF,
1111 Kellis M, Davis CA, Kapranov P, Dobin A, Zaleski C, Schlesinger F, Batut P, Chakrabortty S, Jha S, Lin
1112 W, Drenkow J, Wang Huaien, Bell K, Bell I, Gao H, Dumais E, Dumais J, Antonarakis SE, Ucla C, Borel
1113 C, Guigo R, Djebali S, Lagarde J, Kingswood C, Ribeca P, Sammeth M, Alioto T, Merkel A, Tilgner H,
1114 Carninci P, Hayashizaki Y, Lassmann T, Takahashi H, Abdelhamid RF, Hannon G, Fejes KT, Preall J,
1115 Gordon A, Sotirova V, Reymond A, Howald C, Graison EAY, Chrast J, Ruan Y, Ruan X, Shahab A, Poh
1116 WT, Wei CL, Furey TS, Boyle AP, Sheffield NC, Song L, Shibata Y, Vales T, Winter D, Zhang Z, London
1117 D, Wang Tianyuan, Keefe D, Iyer VR, Lee BK, McDaniell RM, Liu Z, Battenhouse A, Bhinge AA, Lieb
1118 JD, Grasfeder LL, Showers KA, Giresi PG, Kim SKC, Shestak C, Pauli F, Reddy TE, Gertz J, Partridge
1119 EC, Jain P, Sprouse RO, Bansal A, Pusey B, Muratet MA, Varley KE, Bowling KM, Newberry KM,
1120 Nesmith AS, Dilocker JA, Parker SL, Waite LL, Thibeault K, Roberts K, Absher DM, Mortazavi A,
1121 Williams B, Marinov G, Trout D, King B, McCue K, Kirilusha A, DeSalvo G, Fisher KA, Amrhein H,
1122 Pepke S, Vielmetter J, Sherlock G, Sidow A, Batzoglou S, Rauch R, Kundaje A, Libbrecht M,
1123 Margulies EH, Parker SCJ, Elnitski L, Green ED, Hubbard T, Harrow J, Searle S, Parker SCJ, Aken B,
1124 Frankish A, Hunt T, Despacio-Reyes G, Kay M, Mukherjee G, Bignell A, Saunders G, Boychenko V,
1125 Brent M, van Baren MJ, Brown RH, Gerstein M, Khurana E, Balasubramanian S, Lam H, Cayting P,
1126 Robilotto R, Lu Z, Derrien T, Tanzer A, Knowles DG, Mariotti M, Haussler D, Harte R, Diekhans M,
1127 Lin M, Valencia A, Tress M, Rodriguez JM, Raha D, Shi M, Euskirchen G, Grubert F, Kasowski M, Lian
1128 J, Lacroute P, Xu Y, Monahan H, Patacsil D, Slifer T, Yang X, Charos A, Reed B, Wu L, Auerbach RK,
1129 Habegger L, Hariharan M, Rozowsky J, Abyzov A, Weissman SM, Struhl K, Lamarre-Vincent N,
1130 Lindahl-Allen M, Miotto B, Moqtaderi Z, Fleming JD, Newburger P, Farnham PJ, Frietze S, O'Geen H,
1131 Xu X, Blahnik KR, Cao AR, Iyengar S, Kaul R, Thurman RE, Wang Hao, Navas PA, Sandstrom R, Sabo

1132 PJ, Weaver M, Canfield T, Lee K, Neph S, Roach V, Reynolds A, Johnson A, Rynes E, Giste E, Vong S,
1133 Neri J, Frum T, Nguyen ED, Ebersol AK, Sanchez ME, Sheffer HH, Lotakis D, Haugen E, Humbert R,
1134 Kutyavin T, Shafer T, Noble WS, Dekker J, Lajoie BR, Sanyal A, Rosenbloom KR, Dreszer TR, Raney
1135 BJ, Barber GP, Meyer LR, Sloan CA, Malladi VS, Cline MS, Learned K, Swing VK, Zweig AS, Rhead B,
1136 Fujita PA, Roskin K, Karolchik D, Kuhn RM, Wilder SP, Sobral D, Herrero J, Beal K, Lukk M, Brazma A,
1137 Vaquerizas JM, Luscombe NM, Bickel PJ, Boley N, Brown JB, Li Q, Huang H, Sboner A, Yip KY, Cheng
1138 C, Yan KK, Bhardwaj N, Wang Jing, Lochovsky L, Jee J, Gibson T, Leng J, Du J, Harris RS, Song G,
1139 Miller W, Suh B, Paten B, Hoffman MM, Buske OJ, Weng Z, Dong X, Wang Jie, Xi H, Tenenbaum SA,
1140 Doyle F, Chittur S, Penalva LO, Tullius TD, White KP, Karmakar S, Victorsen A, Jameel N, Bild N,
1141 Grossman RL, Collins PJ, Trinklein ND, Giddings MC, Khatun J, Maier C, Wang Ting, Whitfield TW,
1142 Chen X, Yu Y, Gunawardena H, Feingold EA, Lowdon RF, Dillon LAL, Good PJ, Risk B. 2011. A user's
1143 guide to the encyclopedia of DNA elements (ENCODE). *PLoS Biol* **9**.
1144 doi:10.1371/JOURNAL.PBIO.1001046

1145 Neuwirth E. 2022. RColorBrewer: ColorBrewer Palettes.

1146 Nilsson EE, Anway MD, Stanfield J, Skinner MK. 2008. Transgenerational epigenetic effects of the
1147 endocrine disruptor vinclozolin on pregnancies and female adult onset disease. *Reproduction*
1148 **135**:713–721. doi:10.1530/REP-07-0542

1149 Nystrom S. 2023. motif matching, comparison, and de novo discovery using the MEME Suite.

1150 Ohta H, Kurimoto K, Okamoto I, Nakamura T, Yabuta Y, Miyauchi H, Yamamoto T, Okuno Y, Hagiwara M,
1151 Shirane K, Sasaki H, Saitou M. 2017. In vitro expansion of mouse primordial germ cell- like cells
1152 recapitulates an epigenetic blank slate. *EMBO J* **36**:1888–1907. doi:10.15252/embj

1153 Okonechnikov K, Conesa A, García-Alcalde F. 2016. Qualimap 2: advanced multi-sample quality control
1154 for high-throughput sequencing data. *Bioinformatics* **32**:292–294.

1155 doi:10.1093/BIOINFORMATICS/BTV566

1156 Ozgyin L, Erdos E, Bojcsuk D, Balint BL. 2015. Nuclear receptors in transgenerational epigenetic
1157 inheritance. *Prog Biophys Mol Biol*. doi:10.1016/j.pbiomolbio.2015.02.012

1158 Pagès H, Carlson M, Falcon S, Li N. 2023. AnnotationDbi: Manipulation of SQLite-based annotations in
1159 Bioconductor. doi:10.18129/B9.bioc.AnnotationDbi

1160 Patrat C, Okamoto I, Diabangouaya P, Vialon V, Le Baccon P, Chow J, Heard E. 2009. Dynamic changes in
1161 paternal X-chromosome activity during imprinted X-chromosome inactivation in mice. *Proc Natl*
1162 *Acad Sci U S A* **106**:5198–5203. doi:10.1073/pnas.0810683106

1163 Picard Tools - By Broad Institute. n.d. https://broadinstitute.github.io/picard/

1164 Ribeiro E, Delgadinho M, Brito M. 2019. Environmentally Relevant Concentrations of Bisphenol A
1165 Interact with Doxorubicin Transcriptional Effects in Human Cell Lines. *Toxics* **7**.
1166 doi:10.3390/TOXICS7030043

1167 Rio DC, Ares M, Hannon GJ, Nilsen TW. 2010. Purification of RNA using TRIzol (TRI Reagent). *Cold Spring*
1168 *Harb Protoc* **5**:1–4. doi:10.1101/pdb.prot5439

1169 Robinson MD, McCarthy DJ, Smyth GK. 2010. edgeR: a Bioconductor package for differential expression
1170 analysis of digital gene expression data. *Bioinformatics* **26**:139–140.
1171 doi:10.1093/BIOINFORMATICS/BTP616

1172 Robinson MD, Oshlack A. 2010. A scaling normalization method for differential expression analysis of
1173 RNA-seq data. *Genome Biol* **11**:1–9. doi:10.1186/GB-2010-11-3-R25/FIGURES/3

1174 Rodig SJ. 2022. Cell Staining. *Cold Spring Harb Protoc* **2022**:pdb.top099606. doi:10.1101/PDB.TOP099606

1175 Roy SK, Greenwald GS. 1996. Methods of separation and in-vitro culture of pre-antral follicles from

1176 mammalian ovaries. *Hum Reprod Update* **2**:236–245.

1177 Ryan D. n.d. MethylDackel: A (mostly) universal methylation extractor for BS-seq experiments.
1178 https://github.com/dpryan79/MethylDackel

1179 Sambrook J, Russell DW. 2006. Purification of Nucleic Acids by Extraction with Phenol:Chloroform. *Cold*
1180 *Spring Harb Protoc* **2006**. doi:10.1101/PDB.PROT4455

1181 Santos F, Hendrich B, Reik W, Dean W. 2002. Dynamic Reprogramming of DNA Methylation in the Early
1182 Mouse Embryo. *Dev Biol* **241**:172–82. doi:10.1006/dbio.2001.0501

1183 Sanz LA, Kota SK, Feil R. 2010. Genome-wide DNA demethylation in mammals. *Genome Biol* **11**.
1184 doi:10.1186/gb-2010-11-3-110

1185 Schilbert HM, Rempel A, Pucker B. 2020. Comparison of Read Mapping and Variant Calling Tools for the
1186 Analysis of Plant NGS Data. *Plants 2020, Vol 9, Page 439* **9**:439. doi:10.3390/PLANTS9040439

1187 Schindelin J, Arganda-Carreras I, Frise E, Kaynig V, Longair M, Pietzsch T, Preibisch S, Rueden C, Saalfeld
1188 S, Schmid B, Tinevez JY, White DJ, Hartenstein V, Eliceiri K, Tomancak P, Cardona A. 2012. Fiji: an
1189 open-source platform for biological-image analysis. *Nat Methods 2012 97* **9**:676–682.
1190 doi:10.1038/nmeth.2019

1191 Senyildiz M, Karaman EF, Bas SS, Pirincci PA, Ozden S. 2017. Effects of BPA on global DNA methylation
1192 and global histone 3 lysine modifications in SH-SY5Y cells: An epigenetic mechanism linking the
1193 regulation of chromatin modifiying genes. *Toxicol Vitr* **44**:313–321. doi:10.1016/j.tiv.2017.07.028

1194 Sloan CA, Chan ET, Davidson JM, Malladi VS, Strattan JS, Hitz BC, Gabdank I, Narayanan AK, Ho M, Lee
1195 BT, Rowe LD, Dreszer TR, Roe G, Podduturi NR, Tanaka F, Hong EL, Cherry JM. 2016. ENCODE data
1196 at the ENCODE portal. *Nucleic Acids Res* **44**:D726–D732. doi:10.1093/NAR/GKV1160

1197 Slowikowski K, Schep A, Hughes S, Dang TK, Lukauskas S, Irisson J-O, Kamvar ZN, Ryan T, Christophe D,
1198 Hiroaki Y, Gramme P, Abdol AM, Barrett M, Cannoodt R, Krassowski M, Chirico M, Aphalo P. 2023.
1199 ggrepel: Automatically Position Non-Overlapping Text Labels with "ggplot2."

1200 Smith AD, de Sena Brandine G. 2021. Falco: High-speed FastQC emulation for quality control of
1201 sequencing data. *F1000Research* **8**. doi:10.12688/F1000RESEARCH.21142.2/DOI

1202 Song A, Ona J, Osuna C, Phandthong R, Talbot P. 2023. Establishing a Disease-in-a-Dish Model to Study
1203 SARS-CoV-2 Infection During Prenatal Development. *Curr Protoc* **3**. doi:10.1002/CPZ1.759

1204 Song K-H, Lee K, Choi H-S. 2011. Endocrine Disrupter Bisphenol A Induces Orphan Nuclear Receptor
1205 Nur77 Gene Expression and Steroidogenesis in Mouse Testicular Leydig Cells. *Endocrinology*
1206 **143**:2208–2215. doi:10.1210/endo.143.6.8847

1207 Swedenborg E, Rüegg J, Mäkelä S, Pongratz I. 2009. Endocrine disruptive chemicals: mechanisms of
1208 action and involvement in metabolic disorders. *J Mol Endocrinol* **43**:1–10. doi:10.1677/jme-08-
1209 0132

1210 Team BC. 2015. Mus.musculus: Annotation package for the Mus.musculus object.
1211 doi:10.18129/B9.bioc.Mus.musculus

1212 Team TBD. 2021. BSgenome.Mmusculus.UCSC.mm10: Full genome sequences for Mus musculus (UCSC
1213 version mm10, based on GRCm38.p6). doi:10.18129/B9.bioc.BSgenome.Mmusculus.UCSC.mm10

1214 Thomas P, Dong J. 2006. Binding and activation of the seven-transmembrane estrogen receptor GPR30
1215 by environmental estrogens: A potential novel mechanism of endocrine disruption. *J Steroid*
1216 *Biochem Mol Biol* **102**:175–179. doi:10.1016/j.jsbmb.2006.09.017

1217 Tremblay B. 2023. universalmotif: Import, Modify, and Export Motifs with R.

1218 Triche TJ, Weisenberger DJ, Van Den Berg D, Laird PW, Siegmund KD. 2013. Low-level processing of
1219 Illumina Infinium DNA Methylation BeadArrays. *Nucleic Acids Res* **41**:e90–e90.
1220 doi:10.1093/NAR/GKT090

1221 vom Saal FS, Hughes C. 2005. An extensive new literature concerning low-dose effects of bisphenol A
1222 shows the need for a new risk assessment. *Environ Health Perspect*. doi:10.1289/ehp.7713

1223 Wang J, Zhuang J, Iyer S, Lin XY, Greven MC, Kim BH, Moore J, Pierce BG, Dong X, Virgil D, Birney E, Hung
1224 JH, Weng Z. 2013. Factorbook.org: a Wiki-based database for transcription factor-binding data
1225 generated by the ENCODE consortium. *Nucleic Acids Res* **41**:D171–D176.
1226 doi:10.1093/NAR/GKS1221

1227 Wang J, Zhuang J, Iyer S, Lin XY, Whitfield TW, Greven MC, Pierce BG, Dong X, Kundaje A, Cheng Y,
1228 Rando OJ, Birney E, Myers RM, Noble WS, Snyder M, Weng Z. 2012. Sequence features and
1229 chromatin structure around the genomic regions bound by 119 human transcription factors.
1230 *Genome Res* **22**:1798–1812. doi:10.1101/GR.139105.112

1231 Wang T, Pehrsson EC, Purushotham D, Li D, Zhuo X, Zhang B, Lawson HA, Province MA, Krapp C, Lan Y,
1232 Coarfa C, Katz TA, Tang WY, Wang Z, Biswal S, Rajagopalan S, Colacino JA, Tsai ZTY, Sartor MA,
1233 Neier K, Dolinoy DC, Pinto J, Hamanaka RB, Mutlu GM, Patisaul HB, Aylor DL, Crawford GE,
1234 Wiltshire T, Chadwick LH, Duncan CG, Garton AE, McAllister KA, Bartolomei MS, Walker CL, Tyson
1235 FL. 2018. The NIEHS TaRGET II Consortium and environmental epigenomics. *Nat Biotechnol*.
1236 doi:10.1038/nbt.4099

1237 Wickham H, Chang W, Henry L, Pedersen TL, Takahashi K, Wilke C, Woo K, Yutani H, Dunnington D, Posit
1238 P. 2023a. ggplot2: Create Elegant Data Visualisations Using the Grammar of Graphics.

1239 Wickham H, François R, Henry L, Müller K, Vaughan D, Posit Software P. 2023b. dplyr: A Grammar of

Data Manipulation.

Wickham H, RStudio. 2022. stringr: Simple, Consistent Wrappers for Common String Operations.

Wickham H, Vaughan D, Girlich M, Ushey K, Posit Software, PBC. 2023c. tidyr: Tidy Messy Data.

Wöste M, Leitão E, Laurentino S, Horsthemke B, Rahmann S, Schröder C. 2020. Wg-blimp: An end-to-end analysis pipeline for whole genome bisulfite sequencing data. *BMC Bioinformatics* **21**:1–8. doi:10.1186/S12859-020-3470-5/FIGURES/3

Wright K. 2023. pals: Color Palettes, Colormaps, and Tools to Evaluate Them.

Xie Y, Sarma A, Vogt A, Andrew A, Zvoleff A, Al-Zubaidi A, Simon A, Atkins A, Baumer W, Wolen A, Manton A, Yasumoto A, Baumer B, Diggs B, Zhang B, Yapparov B, Pereira C, Dervieux C, Hall D, Hugh-Jones D, Robinson D, Hemken D, Murdoch D, Campitelli E, Hughes E, Riederer E, Hirschmann F, Simeon F, Fang F, Jr FEH, Aden-Buie G, Detrez G, Wickham H, Zhu H, Jeon H, Bengtsson H, Yutani H, Lyttle I, Daniel H, Bien J, Burkhead J, Manton J, Lander J, Punyon J, Luraschi J, Arnold J, Bryan J, Ashkenas J, Stephens J, Hester J, Cheng J, Ranke J, Honaker J, Muschelli J, Keane J, Allaire J, Toloe J, Sidi J, Larmarange J, Barnier J, Zhong K, Slowikowski K, Forner K, Smith KK, Mueller K, Takahashi K, Walthert L, Gallindo L, Hofert M, Modrák M, Chirico M, Friendly M, Bojanowski M, Kuhlmann M, Patrick M, Caballero N, Salkowski N, Hansen NR, Ross N, Mahdi O, Krivitsky PN, Faria P, Li Q, Vaidyanathan R, Cotton R, Krzyzanowski R, Copetti R, Francois R, Williamson R, Mati S, Kostyshak S, Meyer S, Brouwer S, Bernard S de, Rousseau S, Wei T, Assus T, Lamadon T, Leeper T, Mastny T, Torsney-Weir T, Davis T, Veitas V, Zhu W, Wu W, Foster Z, Kamvar ZN, Posit Software P. 2023. knitr: A General-Purpose Package for Dynamic Report Generation in R.

Yan L. 2023. ggvenn: Draw Venn Diagram by “ggplot2.”

Ye J, Coulouris G, Zaretskaya I, Cutcutache I, Rozen S, Madden TL. 2012. Primer-BLAST: a tool to design

1262 target-specific primers for polymerase chain reaction. *BMC Bioinformatics* **13**:134.
1263 doi:10.1186/1471-2105-13-134

1264 You L, Casanova M, Archibeque-Engle S, Sar M, Fan LQ, Heck H d'A. 1998. Impaired male sexual
1265 development in perinatal Sprague-Dawley and Long- Evans hooded rats exposed in utero and
1266 lactationally to p,p'-DDE. *Toxicol Sci* **45**:162–173. doi:10.1006/toxs.1998.2515

1267 Zhou W. 2022. wheatmap: Incrementally Build Complex Plots using Natural Semantics.

1268 Zhou W, Hinoue T, Barnes B, Mitchell O, Iqbal W, Lee SM, Foy KK, Lee KH, Moyer EJ, VanderArk A,
1269 Koeman JM, Ding W, Kalkat M, Spix NJ, Eagleson B, Pospisilik JA, Szabó PE, Bartolomei MS, Vander
1270 Schaaf NA, Kang L, Wiseman AK, Jones PA, Krawczyk CM, Adams M, Porecha R, Chen BH, Shen H,
1271 Laird PW. 2022. DNA methylation dynamics and dysregulation delineated by high-throughput
1272 profiling in the mouse. *Cell genomics* **2**. doi:10.1016/J.XGEN.2022.100144

1273 Zhou W, Triche TJ, Laird PW, Shen H. 2018. SeSAMe: reducing artifactual detection of DNA methylation
1274 by Infinium BeadChips in genomic deletions. *Nucleic Acids Res* **46**:e123–e123.
1275 doi:10.1093/NAR/GKY691

1276